EVAPORATIVE CONVECTION

John C. Berg

University of Washington, Seattle, Washington

and

Andreas Acrivos and Michel Boudart

Stanford University, Stanford, California

Work done at Department of Chemical Engineering
University of California, Berkeley, California

I. Introduction

The convective flow which occurs spontaneously in evaporating liquids is one of the most spectacular performances that nature has hidden from our view. The show may be staged in a lake, in a bathtub, or in a teacup, but it

is rarely visible to the naked eye. Such flows also occur often in distillation, absorption, and extraction in which heat or mass transfer is occurring within or between fluid phases, and all such phenomena may come under the general heading of "natural," "free," or "spontaneous" convection.

The term "convection" was introduced in 1834 by William Prout "to denote a mode of propagation of heat" (by fluid motion), which had been discovered by Count Rumford 40 years earlier (B16). The notion of convection is actually more general, in that mass, or energy in some form other than heat, may be the object of transport. "Natural" and "free" are appended to "convection" to denote movement induced without the performance of external mechanical work on the fluid.

The object of the present review, a case study of evaporative convection, has the purpose of bringing together those aspects of the broader field of "free convection" which are of primary interest to chemical engineers. The specific problem of evaporative convection provides a particularly appropriate vehicle for such a study: first, because it typifies free convection occurring during and as a result of heat or mass transfer in a fluid layer; second, because it involves a fluid-fluid interface which gives rise to important surface phenomena in fluid mechanics; and third, because it provides a needed backdrop for the many experimental studies where spontaneous convection complicates any attempt to elucidate the molecular mechanism of the evaporation process *per se* (K1, P2).

While the specific subject of evaporative convection is at least implicit throughout this review, most of the development centers around simpler related problems, such as that of convection in a fluid layer confined between solid planes, or convection in a fluid layer with a free surface from which no evaporation takes place. Also the review is largely confined to convection in fluid layers sufficiently thin for the thickness itself to be a primary factor relative to the convection phenomena.

A. The Discovery of Evaporative Convection

Cornelius Varley, an English microscope maker, appears to have been the first to notice, in 1836, "motions of extremely curious and wonderful characters in fluids undergoing evaporation" (V1). The motions were observed with the aid of a microscope by incorporating finely divided coal into the drops and films studied. It remained for James Thompson to give the first explanation of the phenomenon, which he provided in a letter to the Royal Society in 1855 "On Certain Curious Motions Observable at the Surfaces of Wine and Other Alcoholic Liquors" (T3). Thompson reported further observations of natural convection during evaporation in an 1882 note "On a Changing Tesselated Structure in Certain Liquids." He had noticed "in a tub of [soapy] water, in

the yard of a roadside inn, a structure showing itself, which appeared remarkable, and excited a good deal of curiosity..." (T4). The superficial soap film, moved about by the underlying currents, had rendered the normally unseen convection visible. Though they are not the earliest record of such phenomena, Thompson's observations are appropriate for introducing the subject of evaporative convection, because they illustrate the two mechanisms by which evaporation sustains natural convection, and because Thompson was apparently the first to give the correct explanation of each mechanism.

What Thompson had seen in his wine glass, and what others had noticed probably since the invention of the beverage, was evaporative convection driven by unbalanced surface tension. In a partially filled goblet of wine, a film of wine wetting the inside surface of the goblet will writhe, shrink into droplets, and run down. Thompson noted that "the tensile force [surface tension] is not the same in different liquids. Thus it is found to be much less in alcohol than in water." He then explained the motions in the evaporating wine films in the following terms:

> "The more watery portions of the entire surface, having more tension than those which are more alcoholic, drag the latter briskly away, sometimes even so as to form a horizontal ring of liquid high up round the interior of the vessel, and thicker than that by which the interior of the vessel was wet. Then the tendency is for the various parts of this ring or line to run together to those parts which happen to be most watery, and so there is no stable equilibrium, for the parts to which the various portions of the liquid aggregate themselves soon become too heavy to be sustained, and so they fall down. . . . The film adhering to the inside of the glass must very quickly become more watery than the rest, on account of the evaporation of the alcohol contained in it being more rapid than the evaporation of the water" (T3).

In contrast to the above mechanism, Thompson suggested a buoyancy mechanism to explain the tesselations in the tub of warm evaporating washwater (T4).

> "The phenomenon seems to be associated essentially with cooling of the liquid at its surface where exposed to the air, when the main body of the liquid is at a temperature somewhat above that assumed by a thin superficial film. A very slight excess of temperature in the body of the fluid above that of the surrounding air is sufficient to institute the tesselated changing structure."

Figure 1 illustrates both phenomena described by Thompson. Actually both mechanisms are operative in both systems, but that of surface tension predominates in shallow layers while that of buoyancy dominates when the

layers are deep. Although this fact can now be demonstrated with certainty, it eluded researchers for over 100 years after Thompson's early observations.

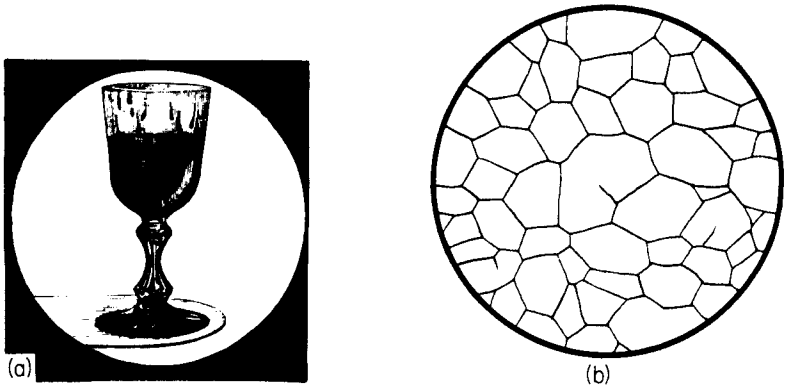

FIG. 1. Thompson's early observations of evaporative convection: (a) the wine-drop phenomenon as observed by Thompson in 1855 (B15) (© 1959 by Educational Services Inc. and reprinted by permission); (b) tesselations observed by Thompson at the surface of a tub of warm soapy water in 1882 (T4).

Just when an evaporating layer goes from "shallow" to "deep" in terms of the mechanism dominating its convection is treated later in this study.

B. THE TWO MECHANISMS WHICH DRIVE EVAPORATIVE CONVECTION

Evaporation activates the *surface tension "engine"* when it causes the surface tension of the liquid right at the surface to exceed the value that would correspond to the bulk liquid beneath. It accomplishes this by removing heat from the surface region, thereby reducing the surface temperature below that of the bulk liquid. For virtually all liquids, surface tension rises as temperature falls (A1); evaporation, by reducing the surface temperature, thus raises the surface tension. Parenthetically this explains numerous reported values for surface tension which are too high (H5).

Any liquid whose surface layer has a tension higher than the equilibrium value corresponding to its bulk composition is potentially unstable, because the potential energy of the surface layer is not at a minimum. Surface tension is defined as the surface free energy per unit area (G1), so that the most stable arrangement for a liquid with a free surface would be the one in which the material of *least* surface tension is placed in the surface layer. Since this is the opposite of the situation encountered in an evaporating liquid, the latter is unstable with respect to surface forces, and tends to exhibit surface tension driven natural convection in seeking to rearrange itself into a more stable configuration.

In addition to the surface tension effect, evaporation activates the *buoyancy*

"*engine*" by causing the density of the liquid near the surface to become greater than that of the bulk liquid beneath when solutions evaporate, both by the depletion of the components of least density from the surface region and by surface cooling. It is possible, then, for evaporation to result in both an "adverse" temperature gradient and an "adverse" concentration gradient, the term "adverse" indicating that the arrangement is potentially unstable.

C. Early Explorations

Early work consisted chiefly of the reported chance observations and rough experiments concerning "spontaneous" fluid motions, which can now be attributed to surface tension, buoyancy, or to a combination of these effects. Evaporation was not the unique generator of spontaneous fluid motion, which was sometimes induced by heating the fluid from below, or by changing the composition in the surface region (by adding a foreign component or by contacting unequilibrated liquid phases with one another).

1. *Surface Tension Driven Convection*

As early as 1686, Heyde observed spontaneous fluid motion when fragments of camphor were placed on olive oil (T6), while Romieu, in 1748, noted the same motion of camphor on the surface of water. Further observations were recorded and argued over until Tomlinson's reviews in 1869 (T6). Tomlinson adopted the explanation first put forth by Carradori in 1794: reaction of camphor particles to the spreading force of a camphor film caused them to "dance," whereas if the camphor were held still, the underlying fluid could be visibly set into motion. Other observations of surface tension convection recorded by 1869 included those of Varley (V1); Thompson (T3,1 T4); Matteuci, in 1833 (cf. T6), concerning the motion of ether laden bits of cork placed on water; Weber, in 1855, concerning evaporating drops of alcohol-water solutions; Tomlinson, in 1864 (T5), concerning the motion of particles of eugenic acid at the surface of water; Bois-Reymond, in 1858; and Lüdtge, in 1869 (cf. T6).

During the 1870's, Carlo Marangoni, who was apparently aware of Carradori's work but not of Thompson's, formulated a rather complete theory of surface tension driven flow (M2, M3). He noted that *flow* could result from surface tension variations as they are caused by differences in temperature and superficial concentration, and that, conversely, variations in temperature and concentration could be induced by an imposed surface flow. Marangoni ascribed several new rheological properties to the surface (notably surface viscosity, surface elasticity, and even surface plasticity), while remarking that perhaps some of these properties could be associated only with surface contamination. Most present-day authors ascribe the first explanation of surface tension driven flow to Marangoni, and term such flow a "Maragoni effect."

2. *Buoyancy-Driven Convection*

Thermal convection, driven by gravity, seems to have been recorded first by Count Rumford in 1797 (R4). After accidentally observing the behavior of fluid in a thermometer he reported:

> "I saw the whole mass of the liquid in the tube in a most rapid motion running swiftly in two opposite directions, up and down at the same time.... Some fine particles of dust had found their way into it and these particles which were intimately mixed with the spirits of wine, on their being illuminated by the sun's beam, became perfectly visible. On examining the motion of the spirits of wine with a lens, I found that the ascending current occupied the axis of the tube and that it descended by the sides of the tube. On inclining the tube a little, the rising current moved out of the axis and occupied the side of the tube which was uppermost, while the descending currents occupied the whole of the lower side of it" (R4).

Rumford went on to explain the phenomenon correctly in terms of the effect of heat on the fluid density: "[Heat] is transported by its particles, these particles being put in motion by the change which is produced in their specific gravity by the change of temperature...."

Some scattered experiments followed those of Rumford but uncovered little new knowledge. Vettin, in 1857, reported convection currents resulting from a point heat source held in a chamber of smoky air (V4). Tyndall, in 1863, and von Bezold, in 1885 (A4), produced varied convection currents in cylinders of water by heating them in various ways. Czermak, in 1893, photographed trajectories obtained with a small heat source placed at the center of a cylindrical vessel of water containing suspended particles (V4). Finally, Guebhard, in 1897 (B6), noted regular patterns on an exposed photographic plate left in a developer bath, due to natural convection induced by evaporation.

3. *The Experiments of Henri Bénard*

At the turn of the century, Henri Bénard, a young French physicist, published the first truly systematic study of natural convection in a horizontal fluid layer (B4, B5, B6). In a horizontal liquid layer heated from below Bénard, sought to measure and to define the most stable steady-state convection currents prevailing under given conditions. He utilized liquid layers only a few millimeters in thickness, initially in an apparatus giving a free upper surface, and of considerable horizontal extent (about 20 cm) so that edge effects could not influence the form of the convection pattern. For these studies,

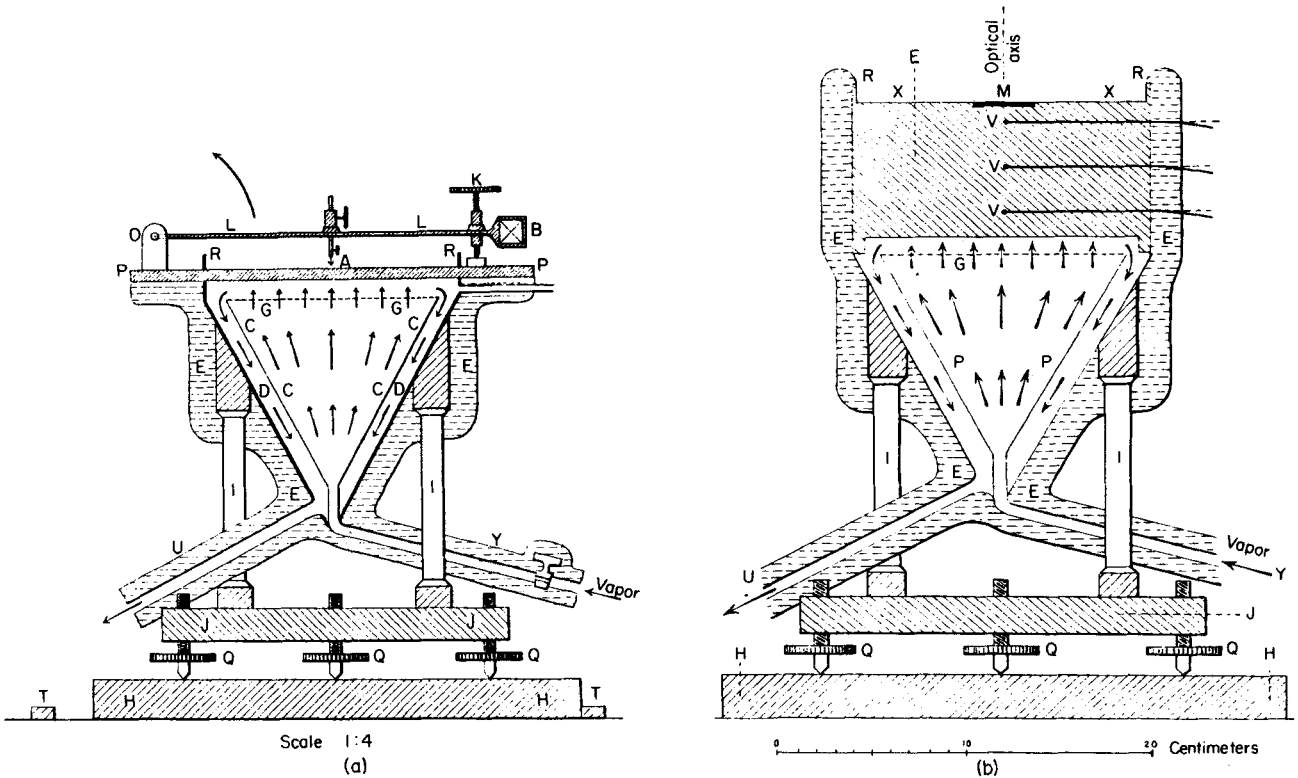

FIG. 2. Bénard's thermal apparatus (B6): (a) shows device for measurement of liquid depth; (b) used for heat flux measurements.

melted spermaceti[1] (cetyl palmitate) at or near 100°C proved to have a viscosity small enough to establish the steady-state regime within a short time and large enough so that this regime was stable toward minute unavoidable perturbations.

From a cylindrical block of iron, Bénard later fashioned a vessel, shown in Fig. 2, 20 cm in diameter and 8 cm thick, with thermocouples placed in the block for measuring vertical heat flux. The bottom of the vessel was an

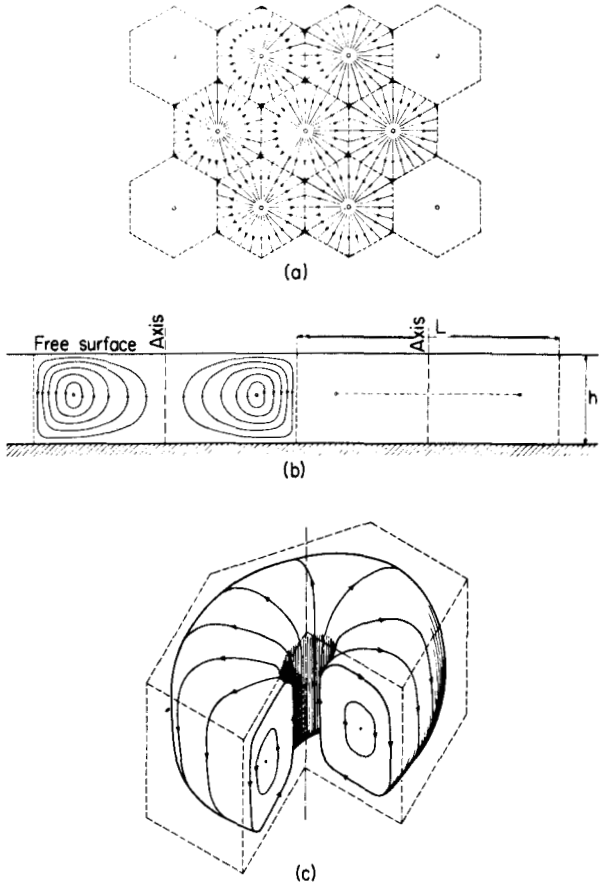

FIG. 3. Steady cellular convection as observed by Bénard (B8) (cf. A4) (courtesy of Ministry of Air, Paris): (a) top view; (b) side view; (c) perspective view.

[1] Bénard experimented with several different liquids and found that volatile liquids (ether at 15°C, alcohol at 50°C) produced rapid, chaotic, permanently unsteady motions. A qualitative description of the currents in evaporating ether was given by Bénard, but the bulk of his report concerns spermaceti.

excellent thermal conductor, and served to maintain the bottom surface (on which steam was condensing) at uniform temperature. The vessel was well insulated around the edges to prevent lateral dissipation of heat. Thermal conditions at the upper free surface were also kept as uniform as possible. The upper face of the metallic block forming the liquid container was dulled and blackened, except for a central area occupied by a flat circular steel mirror of 32 mm diam., cast into the iron "dish," which was used to view the convection.

Two types of procedures (discussed in detail below) were used to study the convection patterns, one employing the incorporation of solid particles into the fluid, and the other optical techniques. The circulation pattern revealed by these is best described with the aid of the drawings shown in Fig. 3 which pertain to the final steady-state convection pattern. The liquid rose in a series of vertical streams located at the centers of polygons, which, in this limiting stable state, constituted a network of regular hexagons. Upon reaching the surface, the liquid of the ascending streams spread radially from the centers toward the edges of the hexagons and then descended to the floor of the vessel where it flowed along the floor inward to the centers of ascension. Unsteady-state flow patterns which always preceded the steady patterns, were qualitatively similar to those of the final regime, and exhibited a polygonal structure (polygons had from four to seven sides) with liquid ascending at the center of the cells and descending along the partitions.

Bénard also showed that the character of the roughly cellular pattern which was initially established would depend upon any overall fluid motion that might have been present at the time of the inception of the cellular vortices. For example, if originally the fluid were in a slight translational motion, the

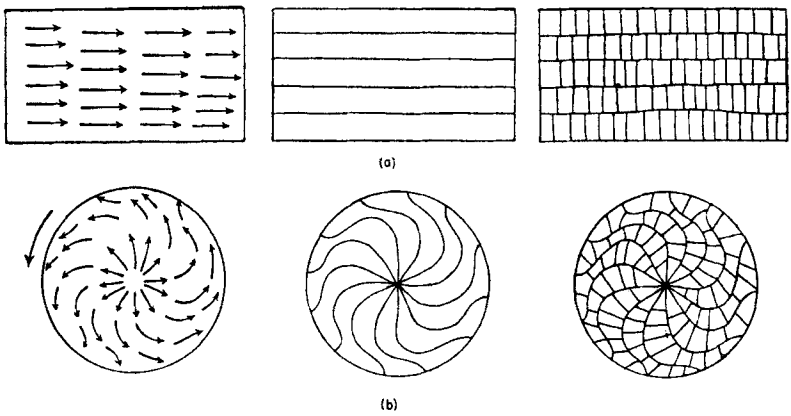

Fig. 4. The effect of fluid motion present at the inception of cellular convection (B4): (a) the effect of initial translational motion; (b) the effect of initial rotational motion.

cellular vortices would appear as shown in Fig. 4(a), whereas an initial rotational motion produced an unsteady pattern of the type shown in Fig. 4(b). In all cases, however, the final permanent regime was the same: a network of regular hexagons.

The chief results of Bénard's work are as follows:

(*1*) Melted spermaceti, and other nonvolatile liquids of like viscosity, exhibit a permanent convective regime. This regime is preceded first by a brief period in which no convection can be discerned, followed by a temporary flow structure comprising irregular polygons of varying size and number of sides. The permanent regime is established within a few minutes. If the liquid is volatile or has a very low viscosity, no stationary state is attained.

(*2*) Liquids of slight volatility can be made to exhibit a pseudopermanent regime, but the continually changing depth of the structure prevents the formation of a rigorously permanent regime. In a typical nonpermanent regime, evaporating ether, the "cells" seem to undergo a random translational motion, constantly growing and diminishing by exchange with their neighbors, and sometimes congregating in chains or colonies.

(*3*) Regardless of the thickness of the liquid layer (which was varied between 0.440 and 1.200 mm) the most stable convection pattern is a network of regular hexagons whose center-to-center distance is 3.2 times the thickness. In the nonpermanent regime, also, the cell size is proportional to the thickness.

(*4*) At constant temperatures, the ratio of cell size to layer thickness is unchanged by varying the heat flux as much as threefold.

(*5*) As the temperature is changed, the cell size reaches a minimum somewhere between 50 and 100°C; the temperature giving this minimum rises as the liquid-layer thickness is decreased.

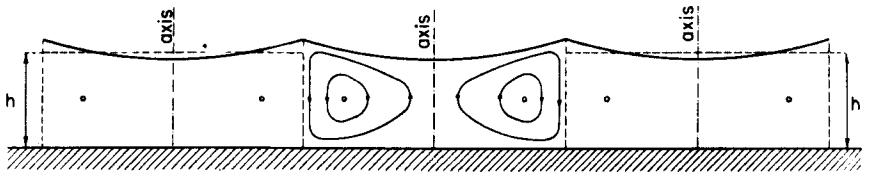

FIG. 5. Exaggerated elevation view of surface deformation caused by cellular convection (A4) (courtesy of Ministry of Air, Paris).

(*6*) The difference in surface elevation within the cellular vortices is of the order of 1 μ. Over the range of thicknesses studied, it varies inversely with layer thickness, and directly with temperature (see Fig. 5). Along the surface, the center of the cell was found to lie below the cell boundary.

(*7*) At a given temperature and heat flux, fluid velocity in the cells is independent of layer thickness, but directly proportional to the heat flux.

(*8*) Most important, but mentioned only casually by Bénard, there is

generally a minimum heat flux below which no convection seems to occur despite the "adverse" density profile. In terms of present knowledge, Bénard found that, during the preconvective period the viscosity and the thermal conductivity of the fluid are capable of damping and destroying small mechanical and thermal disturbances so that no convection results.

From these findings, Bénard established the two fundamental facts concerning natural convection (C2); "First, a certain critical temperature gradient has to be exceeded before instability can set in; second, the motions that ensue on surpassing the critical temperature gradient have a cellular pattern." His first conclusion opened the question as to when and under what conditions natural convection would occur, while the second provided new insight into a whole array of diverse phenomena: cellular cloud patterns (M4), the polygonal distribution of rocks in certain arctic regions (L8), lunar craters (B7), the cells of living tissue (B4), uneven drying of paint films (B3), regular patterns formed by photographic developer on films and plates (B10), cellular patterns formed during the solidification of glass (cf. S6), and sun spots (B11), to name but a few.

As will be shown below, Bénard's work also provided for many years ahead the experimental foundation for the study of cellular convection. His dramatic results inspired the work of many others, chief among them a group of French experimentalists, and a number of English theoretical physicists led by Lord Rayleigh.

In this review, we shall begin by discussing the experimental techniques which have been used to study either or both of the above two aspects of the problem. Stability criteria will be treated next. Finally, a thorough investigation of the cellular morphology will be given, with particular emphasis on evaporative convection.

II. Experimental Methods

Many methods have been applied to the experimental investigation of convection in horizontal fluid layers, some best suited for determining the stability criterion, and others designed to study the fully developed convective flow patterns. Three principal types of experimental methods have been employed: (*1*) suspended particle methods; (*2*) optical methods; and (*3*) thermal methods. In addition, a few special techniques have been introduced which fall outside the above categories.

A. Suspended Particles

Perhaps the most obvious technique for visualizing flow is to incorporate, into the fluid, small solid particles whose motion can be seen and photographed. It was the chance presence of such suspended solids that led to the

initial discovery of thermal convection. Later, Bénard employed the method to the fullest extent. Particles denser than the liquid medium were first deposited at the bottom of the layer and then swept by the centripetal cellular currents into small piles, whose regularity and spacing revealed both the dimensions of the cells and their geometry in the steady state. The unsteady convection patterns preceding the steady state could also be traced by following the movement of the small piles, which in this case were drawn into lines that moved about with the shifting, expanding, and contracting of the cellular vortices. Similarly, particles lighter than the fluid, such as lycopodium powder, were used by Bénard to visualize the cell boundaries, since the floating particles, swept radially outward from the cell centers, concentrated along the cell partitions and eventually at the ternary junctions of the hexagonal cells.

The behavior of fine particles having a density equal to that of the fluid, or of particles of colloidal size, is somewhat more complex. When a heated solid body is immersed in a fluid containing such particles, there is formed around the hot surface a thermal boundary layer which is completely free of such particles, and which customarily has a thickness of the order of 0.1 mm. The important fact for visualization purposes is that all the closed streamlines passing through this layer remain free of particles throughout their course; hence, the torus which forms the cell becomes enveloped in a particle-free envelope that renders it clearly visible. Bénard first photographed this pattern by directing light up through the heated glass bottom of the vessel, but since glass is a relatively poor thermal conductor, a completely steady convection was not achieved under these conditions. Bénard then replaced the glass with a metallic bottom, used highly reflective solid particles, and directed a beam of light onto the cellular layer. Flake-like particles, which aligned in the direction of the flow, were found best for this purpose; Bénard obtained good results using powdered aluminum, graphite, and the scales from butterflies' wings!

Subsequent investigators using the method of suspended particles have improved little upon Bénard's techniques. Volkovisky (V3) used aluminum particles to study the circulation in thin films of liquid, which was drawn up by surface tension forces onto a cold flat plate dipping into the liquid. Bell (B3) studied the flotation of pigment particles in drying paint films. Aluminum particles were used by Muller to study convection during the evaporation of thin layers of acetone (L2); and recently Linde (L4) employed them to study convection in thin *vertical* fluid layers, confined between parallel glass plates, undergoing gas absorption and desorption. Jarvis (J1) sprinkled talcum particles on a layer of evaporating water in order to trace convection patterns which were sometimes induced by blowing nitrogen gas against the surface. Also, many investigators used entrained smoke to follow convective movements in gaseous layers (A4, C1, S7, S13).

Suspended particles furnished a means both of viewing the developed flow patterns and of detecting the onset of convective instability, but the method is open to question regarding the extent to which the particles affect the phenomenon. Indeed, in certain experiments (C1, S13), the smoke-gas suspension had sufficiently different properties from those of the pure gases to produce anomalous stability results. Bénard, recognizing this inherent dilemma in the use of solid particles, devised optical techniques for following the fluid motion in detail without introducing any foreign objects.

B. Optical Methods

A fluid layer undergoing thermal convection, or convection due to mass transfer, is optically nonuniform; its refractive index, being a function of temperature and of composition, varies from point to point. As a consequence, light rays passing through the fluid are deflected in a manner which depends on the refractive index variation, and therefore on the distribution of temperature, concentration, or both. Thus, optical techniques may be based on analyzing the behavior of light refracted by the medium. If the fluid layer undergoing convection has a free surface, there is also a free-surface relief that mirrors the convection going on beneath it, which may be studied by analyzing the deflections of light reflected from the surface. Both refracted and reflected light are thus used. They may be analyzed by three different experimental methods, each yielding somewhat different information concerning the convecting medium, and each subject to a great number of variations: (1) interferometry; (2) the schlieren method; and (3) the direct-shadow method.

1. *Interferometry*

The principles of the interferometric method are well known; the subject is generally discussed in beginning physics texts, to illustrate the wave character of light. When two beams of light originating from the same source are made to overlap, either by inclining or by lengthening one beam relative to the other in the region where they cross, their corresponding rays generally are no longer in phase with one another. Thus a plane surface that intercepts the beams in their region of crossing will be illuminated with a pattern of interference fringes.

Two types of interferometers, Fabry–Pérot and Mach–Zehnder, have been applied to the study of convection in horizontal fluid layers.

The Fabry–Pérot type used by Bénard, which produces "fringes of equal thickness," is shown schematically in Fig. 6. Monochromatic light from a source S is collimated by the lens L and is directed vertically onto the

flat horizontal glass plate G. Here some light is reflected.[2] The rest, transmitted by G, passes through the air film between the glass and the liquid layer, and is then partially reflected at the liquid surface F; the remaining part of the light passes through the liquid layer and is completely absorbed at the bottom surface which is dulled and blackened. If n_G and h denote,

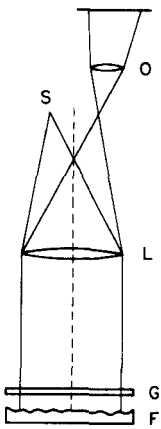

FIG. 6. Schematic drawing of the Fabry–Pérot interferometer of the type used by Bénard to obtain contour lines for the free surface of a liquid undergoing thermal convection.

respectively, the refractive index and the thickness of plate G, and if at a given horizontal position the separation between plate G and the liquid surface F is d, the two optical components of the ray differ in length by $(2d + n_G h)$. "Constructive interference," producing a bright fringe, occurs when this difference in path length is an integral number of wavelengths, both ray components having undergone a phase reversal upon reflection. In constructive interference, those points having fluid elevations such that the air film thickness is d will form bright contour lines. A sequence of contour lines is produced for a sequence of fluid elevations differing by one-half wavelength of light, i.e., a fraction of a micron. Figure 7 shows a schematic drawing of such contour lines as obtained by Bénard for the case of perfectly regular hexagonal convection cells. (The direction of the elevation changes, i.e., whether cell centers were relatively elevated or depressed, had to be determined by other means.)

The Mach–Zehnder interferometer, shown schematically in Fig. 8 and often used to study flow patterns in wind tunnels, has recently been employed

[2] Strictly, there is reflection at both surfaces of G; but since these surfaces are perfectly parallel, the components emerging from them have the same phase relationship for all rays, and contribute in no way to the formation of contour lines.

to determine temperature profiles in fluid layers heated from below (J6). Monochromatic light from the source S is collimated by the lens L and is directed toward the partially silvered mirror M which divides the incident light into two beams, 1 and 2. Plane mirrors M_2 and M_3 direct the two beams to the partially silvered mirror M_4 where they are recombined, part of beam

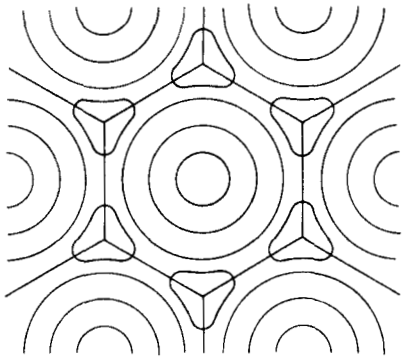

FIG. 7. Contour lines of the type obtained by Bénard for the free surface of a hexagonal convection cell using the Fabry–Pérot interferometer.

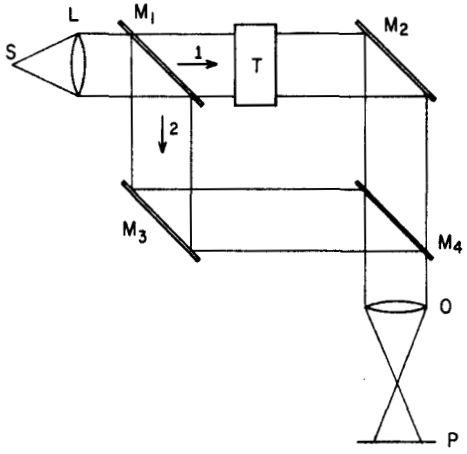

FIG. 8. Schematic drawing of the Mach–Zehnder interferometer.

2 being lost by reflection and part of beam 1 being lost by transmission at M_4. By proper adjustment of M_2 and M_3, the beams emerging from M_4 are inclined slightly to one another so that the objective lens O will project a uniform system of fringes on the photographic plate or viewing screen P. The light beams are widely spaced, so that a test section T may be inserted

in one beam without disturbing the other. Variations in refractive index within the test section will cause variations in the optical path length for the different rays of beam 1, resulting in a shift in the location of the interference fringes. The extent of fringe shift may then be related quantitatively to the refractive index distribution in the test section.

Two factors distinguish interferometry from the other optical methods to be discussed. Interferometry provides data related directly to the elevation or the refractive index of the liquid layer; and it yields data that are generally quantitative.

2. *Schlieren Method*

Schlieren methods provide the most commonly used procedure for investigating convective flow in a horizontal fluid layer. ("Schlieren," a German word, means "streaks.") In contrast to interferometry, this method often is only qualitative. The schlieren technique produces, on the photographic plate or viewing screen, light-intensity variations that are proportional to the *gradient* of refractive index of the medium (or, if the surface relief is under study, to the *slope* of the free surface). The basic principle of the method is that a ray of light passing through the medium in question (or reflected from the surface) undergoes an angular deflection directly proportional to the refractive index gradient (or to the slope of a reflecting surface) at each point along its path. The deviations of the ray are then monitored. The technique was invented by August Toepler in 1864, and the many variations to which it has been subjected are discussed extensively by Holder and North (H4), Schardin (S3), and others (B2).

The simple "two-mirror" arrangement, Fig. 9, serves to illustrate the

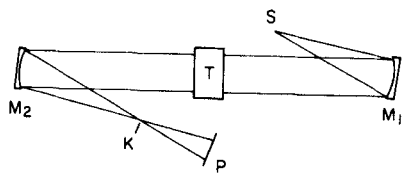

FIG. 9. Schematic drawing of a two-mirror schlieren system.

essential principles. Light from a small source S of well-defined shape is collimated by the parabolic mirror M_1, and is passed through the medium under study. Here some rays may undergo angular deflections, small enough to permit the rays to be gathered and refocused at K by the parabolic mirror M_2. Each of the light rays at T contains light from all points of the source S; so that, upon leaving M_2, each of these independent rays is capable of producing an image of the source S.

If a ray experiences no deflection upon traversing this test section, the light-source image it forms will be located precisely at the point where the optical axis of the system intersects the focal plane K. It follows that, if none of the rays experience deflection, all of the source images will be superimposed in the same spot, forming a clear bright undistorted image of the light source. However, if a particular ray is deflected, its image of the light source in the focal plane K will lie away from the optical axis (see Fig. 10). Now,

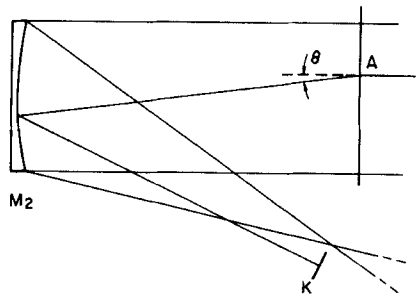

FIG. 10. Sketch showing the blockage of a light ray in a schlieren system. Deflected in the test section, the light ray emerging from A will never reach the viewing screen because it is blocked by the knife edge K.

beyond the focal plane of M_2, a viewing screen P is positioned so that an image of the test section is brought to focus upon it, regardless of the extent to which it is deflected. It is important to note that a ray piercing the test section will be brought to rest at the corresponding point in the *image* of the test section.

Thus there is a point-to-point correspondence between the test section and its image on the viewing screen, regardless of the deflections of the various rays. The ray deflections are rendered visible on the screen by blocking part of the light from reaching the screen with a diaphragm in the focal plane of M_2, so that points in the image corresponding to such rays appear dark. Often the diaphragm is a simple knife-edge K oriented to intercept a fraction of the light in the focal plane of the schlieren mirror, M_2, as shown in Fig. 10. If the knife edge is horizontal, rays deflected upward produce bright spots in the image, rays deflected downward produce dark spots, and rays deflected to the left or right remain unaffected. Correspondingly, the light intensity of the image varies in accordance with the sign and the magnitude of the vertical component of the refractive index gradient in the medium. Therefore, since these gradients are due to temperature or composition gradients, the schlieren patterns can be used to follow the flow in a system where the temperature or composition varies with position.

Bénard used the schlieren method (although not by this name) to obtain

photographs of the surface relief of thin liquid layers undergoing convection, where the light ray underwent deflections proportional to the slope of the surface at the point of incidence. Sellin (S8) has used a reflecting schlieren system to follow surface depressions due to turbulent vortices in forced convection. Linde (L4) has recently employed a schlieren technique (as well as suspended particles) to study spontaneous convection in a liquid confined between vertical glass plates, into which various gases were being absorbed. Orell and Westwater (O2, O3) have used a microscopic schlieren system to study convection during liquid–liquid mass transfer. Spangenberg and Rowland (S10) employed a two-mirror schlieren system to photograph convection in a deep tank of evaporating water. Berg (B12) used such a system to photograph evaporative convection in water, several organic liquids, and several binary solutions.

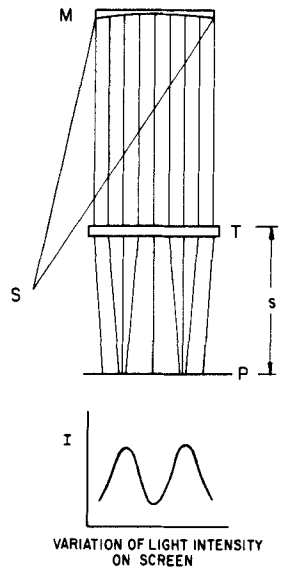

FIG. 11. A schematic drawing of the direct-shadow method showing formation of the shadow image of the liquid layer T on the screen P. It is evident that the nature of the distribution of the light intensity I depends to a large extent on the distances from the test section to the screen.

3. *Direct-Shadow Method*

The direct-shadow technique is probably the simplest in principle, but is subject to the greatest variation. As with the schlieren method, this technique when applied to the study of liquids generally yields only qualitative information. In contrast to the preceding methods, the direct-shadow technique detects differences from point to point in the *second* derivative of the surface

elevation with respect to the horizontal axis (i.e., the surface curvature) or, for a refracted light beam, differences in the divergence of the refractive index gradient.

Direct-shadow optics are much the same as for a schlieren system, but, as shown in Fig. 11, without the schlieren mirror or lens and the diaphragm knife edge. An image showing refractive index variations in the medium under study will result only if these variations produce beams that are either converging or diverging, i.e., if adjacent rays traversing the medium T are deflected by different amounts. It was noted above that a light ray is deflected through an angle directly proportional to the refractive index gradient. Hence, in the direct-shadow image, the light intensity at a certain point on the screen will be inversely proportional to the *divergence* of the refractive index gradient at the corresponding point in the test section. Figure 11 also shows that the intensity is inversely proportional to the distance of the viewing screen from the test section.

Bénard employed two variations of the direct-shadow method, using reflected light to obtain photographs of free-surface relief during convection. In particular because the free surfaces of his convection cells were essentially basins separated by ridges, from the optical standpoint they simulated concave mirrors separated by cylindrical convex mirrors. By adjusting the position of the viewing screen, as shown in Fig. 12, the cell centers could be

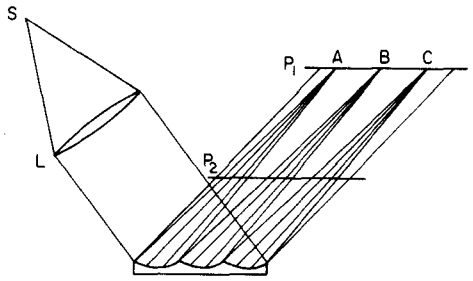

FIG. 12. Diagrammatic sketch of Bénard's direct-shadow system for locating the cell centers and cell partitions on the surface of the liquid. With the viewing screen at P_1, the cell centers appeared to be bright spots, A, B, and C on a dark background, whereas, when the screen was moved closer to the liquid, as at P_2, the image became one of dark lines on a bright background. Bénard's apparatus was actually somewhat different than shown, but the diagram illustrates its important features.

made to appear as bright spots A, B, and C on a dark background (at position P_1); also, the cell partitions could be brought into focus as dark lines on a bright background by moving the screen closer to the liquid (as at P_2). Bénard used these two focal distances to determine the radius of curvature of the concave cell surfaces. The second variation of the direct-shadow technique

involved projecting a rectangular grid onto a screen with light which was reflected from the free surface of the liquid, so that deformations in the grid image could be related to the curvature of the free surface.

The direct-shadow method has been employed in the study of free convection by many authors following Bénard, and unfortunately has often been mislabelled as a "schlieren" method. Levengood (L2) in a study of evaporative convection in pools of methyl alcohol, and Hickman (H2) in a study of surface behavior of boiling liquids, used modifications of Bénard's deformed grid technique.

Saunders, Fishenden, and Mansion (S2) developed a shadow technique in which the image of a long slit, or group of slits, illuminated by a carbon arc point source located several meters behind these slits was projected laterally through a liquid layer onto a screen. The deformations in the slit image were related, through the refractive index, to the temperature variations surrounding vertical and horizontal plates immersed in various fluids. Schmidt and Milverton (S4), Schmidt and Saunders (S5), and later Silveston (S9), used the technique for detecting the onset of convective instability in horizontal fluid layers heated from below.

A summary of the three optical techniques, listing the specific quantities to which each method is sensitive, is given in Table I.

TABLE I

OPTICAL METHODS FOR THE INVESTIGATION OF FREE CONVECTION

Method	Sensitive to what property		Remarks
	Reflected beam	Refracted beam	
Interferometry	Free surface elevation, i.e., h	Refractive index, n	Best method for obtaining quantitative profiles of temperature or concentration
Schlieren	Free surface slope, i.e., grad h^a,	Refractive index gradient, grad n^a	Best method for qualitative observations of convective flow patterns
Shadow	Free surface curvature, div grad h	Divergence of refractive index gradient, div grad n	Simple to construct; sometimes yields quantitative results

[a] This, of course, refers to that component of the gradient which is perpendicular to the edge of the diaphragm.

A good review of all three optical methods, although oriented to wind tunnel work, is given by Holder and North (H4).

C. Thermal and Other Methods

Although the optical methods are clearly superior to use of solid particles in studying free convection, neither technique proves adequate for determining quantitatively the threshold conditions for convective instability. This is so because the precise point at which convection is first detected is always somewhat arbitrary when based on human observations. To remedy this situation, Schmidt and Milverton (S4) assumed that the onset of convection would be indicated by a sudden change in the overall heat transfer coefficient to the fluid; by measuring the heat transfer across a fluid layer confined between parallel horizontal plates, the lower of which was always maintained at the higher temperature, they were able to observe a striking increase in the slope of the heat-transfer rate plotted against temperature difference whenever the latter reached a particular value. This criterion for the onset of convection was both clear-cut and reproducible, and they interpreted it as indicating that the mechanism of pure heat conduction had given way to a combination of conduction with convection. Subsequently, the Schmidt–Milverton thermal technique was used successfully by others (S5, S9).

Other thermal methods for the study of natural convection have employed temperature probes placed at various positions within the fluid layer. Such methods provide a means of studying three-dimensional effects and are thus particularly appropriate for investigating deep fluid layers. Jarvis (J1, J2) measured liquid temperatures in and about the surface of evaporating water by means of a thermistor probe and detected the presence or absence of evaporative convection by the presence or absence of rapid temperature fluctuations at given points near the surface. Spangenberg and Rowland (S10) measured temperature profiles during evaporative convection with a thermopile. Ewing and McAllister (E1) and later Jarvis (J1) used an infrared radiometer to determine the surface temperature of water during evaporation, but no direct measure of the convection phenomena was obtained in this way.

In addition to the foregoing methods, other highly specialized techniques have also been used occasionally to investigate the cellular structure of free convection. For example, Mysels (M5) has employed the color change produced in a filter paper impregnated with cobaltous chloride and held just above the surface of evaporating water, to detect differences in the evaporation rate from different areas of the surface. Earlier, Dauzère (D1) had

quickly solidified a liquid layer undergoing cellular convection, so as to measure the surface deformations at leisure.

III. Work of Lord Rayleigh; Hydrodynamic Stability Analysis

A. Rayleigh's Approach

1. *The Problem of Buoyancy-Driven Convection*

In 1916, when more than 70 years old, Lord Rayleigh (John William Strutt) published his famous paper "On Convection Currents in a Horizontal Layer of Fluid, When the Higher Temperature Is on the Under Side," which he presented as "an attempt to examine how far the interesting results obtained by Bénard in his careful and skilful experiments can be explained theoretically" (R1). Recalling the theoretical predictions he had made earlier regarding the disintegration of liquid jets into droplets, Rayleigh sought to predict by means of small-disturbance analysis the "disintegration" of a quiet layer of liquid when heated from below into cellular vortices.

It was known that jets about to disintegrate first become wavy or "varicose," then break up into a string of equal-sized detached masses that form droplets. Similarly, the experimentally observed regular cellular pattern in free convection suggested that the displacements (or velocities, etc.) resulting from the introduction and growth of disturbances would be spacially periodic, and that the different modes by which a system would fall away from an unstable equilibrium could be characterized in terms of one, two, or three time-independent wavelengths.

In the case of a liquid jet, a growing disturbance could be expressed in terms of a single wavelength which ultimately manifested itself as the wavelength of the observed varicosity preceding the disintegration of the jet. The problem of the unstably heated infinite layer of fluid was similar, except that the disturbance components, distributed over the horizontal plane, required *two* wavelengths for their description. Rayleigh sought to predict the dimensions of the Bénard cells by formulating his problem first in terms of an inviscid fluid analysis which was then extended to include viscosity.

The expected result, instability whenever the fluid density increased upward, proved true when the viscosity was neglected. But when viscous effects were taken into account Rayleigh discovered a thoroughly stable regime in which the density was *greater* at the top, as had been observed by Bénard. Although the problem of locating the threshold of convective instability eventually eclipsed the original problem of finding the preferred wavelengths, both pieces of information emerged from Rayleigh's solution which thus

constitutes one of the few completely solved problems of hydrodynamic stability.

2. *Basic Concepts of Hydrodynamic Stability Analysis*

Although hydrodynamic stability has been thoroughly reviewed by Lin (L3) and by Chandrasekhar (C3), some general comments on the subject are appropriate at this point. Rayleigh's problem, merely one in this general class, is concerned with the stability of an initial "flow regime" in which there is no flow.

To determine the stability of a given steady-state flow to infinitesimal disturbances, we examine first the fate of such disturbances after they first arise. If they decay with time, the regime is said to be *stable*; if they grow with time, the regime is said to be *unstable*.

The mathematical formulation of such a problem begins with the statement of the appropriate equations of change. In Rayleigh's problem, these were the equations of motion, the equation of continuity, and the equation of thermal-energy conservation, together with an appropriate equation of state. In their most general form, these equations are

$$\partial\rho/\partial t + \operatorname{div}(\rho\mathbf{u}) = 0 \qquad \text{(continuity equation)} \tag{1}$$

$$\rho\, D\mathbf{u}/Dt = \rho\mathbf{f} - \operatorname{grad} p - (\tfrac{2}{3})\operatorname{grad}(\mu \operatorname{div}\mathbf{u}) + \operatorname{div}(\mu \operatorname{def}\mathbf{u}) \qquad \text{(equation of motion)} \tag{2}$$

$$\rho\, D(c_v T)/Dt = \operatorname{div}(k \operatorname{grad} T) - p \operatorname{div}\mathbf{u} + (\mu/2)(\operatorname{def}\mathbf{u})\cdot(\operatorname{def}\mathbf{u}) - (\tfrac{2}{3})\mu(\operatorname{div}\mathbf{u})^2 \qquad \text{(energy equation)} \tag{3}$$

$$\rho = \rho_0[1 - \alpha(T - T_0)] \qquad \text{(equation of state)} \tag{4}$$

where

c_v = heat capacity at constant volume,
$\mathbf{f}$ = body force, per unit mass of fluid,
k = thermal conductivity,
T = temperature,
T_0 = reference temperature,
t = time,
$\mathbf{u}$ = fluid velocity,
def $\mathbf{u}$ = grad $\mathbf{u}$ + (grad $\mathbf{u}$) transpose
D/Dt = substantial derivative,
α = volumetric coefficient of thermal expansion,
ρ = density,
ρ_0 = fluid density at $T = T_0$, and
μ = viscosity.

We now set

$$\mathbf{u} \equiv \hat{\hat{\mathbf{u}}} + \hat{\mathbf{u}}; \qquad T \equiv \hat{\hat{T}} + \hat{T}, \text{ etc.} \tag{5}$$

where $\hat{}$ denotes the intital steady-state value of the variable and $\hat{}$ denotes its perturbation. In Rayleigh's problem, the vertical axis is generally designated as z, the origin is located in the bottom surface of the fluid layer, and the unperturbed temperature profile is assumed to be linear, so that

$$\hat{\hat{T}} = \hat{\hat{T}}_0 - \beta z \tag{6}$$

where $\beta \equiv -d\hat{\hat{T}}/dz$ is minus the steady-state linear temperature gradient and T_0 is the temperature at the bottom surface.

Gravity is considered to be the only body force, and therefore

$$\mathbf{f} = -g\mathbf{e}_z \tag{7}$$

where $\mathbf{e}_x$, $\mathbf{e}_y$, $\mathbf{e}_z$ are unit vectors in the x, y, and z directions, respectively.

These expressions are now substituted into Eqs. (1)–(4) which are then linearized by supposing the perturbations to be very small. Thus, in terms of the perturbed quantities $\hat{\mathbf{u}}$, $\hat{T}$, etc. (but dropping the superscript $\hat{}$), we obtain

$$\text{div } \mathbf{u} = 0 \tag{8}$$

$$\partial \mathbf{u}/\partial t = g\alpha T\mathbf{e}_z - \text{grad } p + \nu \text{ div (grad } \mathbf{u}) \tag{9}$$

$$\partial T/\partial t - \beta \mathbf{u} \cdot e_z = \kappa \text{ div (grad } T) \tag{10}$$

where $\kappa \equiv k_0/\rho_0 c_{v0}$ is the thermal diffusivity, and $\nu = \mu_0/\rho_0$ the kinematic viscosity. The derivation of the above linearized perturbation equations from the set of general equations (1)–(4) is carried out in detail by Chandrasekhar (C3).

3. *The Solution of Rayleigh's Problem*

In Rayleigh's words, "We now assume in the usual manner that the small quantities are proportional to $e^{ilx} e^{imy} e^{qt}$," where the "small quantities" are of course the disturbance variables or perturbation quantities in Eqs. (8–10). In view of the linearity of the governing equations, we can express any one of these, say T, in terms of its Fourier transform

$$T(x, y, z, t) = \int_{-\infty}^{\infty}\int T^*_{l,m}(z)\, e^{ilx} e^{imy} e^{q(l,m)t}\, dl\, dm \tag{11}$$

(where an asterisk denotes dependence on z only) provided that the system is infinite in extent in both the x and the y directions. For finite systems a somewhat different formulation is required (P3).

The different modes of the disturbance can then be thought of as giving rise to the various terms in Eq. (11), and refer to the different horizontal

patterns by which the unstable equilibrium may disintegrate. We note that "l" and "m" are wave numbers referred to some one pair of mutually perpendicular axes in the horizontal plane, so that use of Eq. (11) restricts the theoretical treatment to rectangular cells with two-dimensional roll cells being included as a limiting case. As we shall see presently, the stability analysis yields a "critical" value for the quantity $a^2 \equiv l^2 + m^2$, but not for the ratio l/m.

The particular boundary conditions to be satisfied at the top and bottom surfaces of the fluid layer determine the form of the z dependence of the solution, i.e., the functions $T^*(z)$, $\mathbf{u}^*(z)$, etc. These are then used to locate the "marginal state" and thereby the "critical" point of the system, by recalling that the parametric space (defined by the parameters of the differential equations) contains both stable and unstable regions and hence a boundary between these two domains which is termed the "marginal state" or the "state of neutral stability." Furthermore, in most stability problems, all the parameters of the system are fixed *a priori* except for one which is allowed to vary continuously over some range; this one parameter then possesses some "critical" value that separates the stable from the unstable portions of the range.

Strictly speaking, then, the stability analysis is limited to locating the marginal state, that is, the region in parameter space where the real part of the growth constant q is zero. The state of marginal stability can be, of course, one of two kinds, depending on whether or not $q^{(i)}$ (the imaginary part of the growth constant) is zero.

Thus, if $q^{(i)}$ is zero, the marginal state is *stationary* in that the amplitudes of the disturbance variables exhibit no time dependence; whereas if $q^{(i)}$ is not zero[3], the amplitudes of the disturbances in the marginal state are periodic in time.

To locate the marginal state, expressions such as Eq. (11) are substituted into Eqs. (8–10). The real part of q is then set equal to zero, and the resulting set of linear homogeneous ordinary differential equations is solved, subject to the appropriate boundary conditions which are also generally homogeneous.

As a rule, a great deal of simplification in the equations results if $q^{(i)}$ is assumed equal to zero at the marginal state, an assumption termed "the principle of exchange of stabilities," which is frequently invoked in stability analyses without any attempt to justify it rigorously. Rayleigh himself showed that this step was correct for his problem, for the one set of boundary conditions that he considered; Pellew and Southwell (P3) extended the proof to other boundary conditions as well. Of course, the failure to account for oscillatory marginal states when these are indeed possible, amounts actually

[3] Actually, nonzero values of $q^{(i)}$ will appear as conjugate pairs.

to solving an incorrect set of governing equations, thereby computing an incorrect set of conditions for the state of neutral stability.

When the viscosity is neglected, Eqs. (8–10) reduce to

$$\frac{\partial u_x}{\partial \tilde{x}} + \frac{\partial u_y}{\partial \tilde{y}} + \frac{\partial u_z}{\partial \tilde{z}} = 0 \tag{12}$$

$$\left.\begin{aligned} \frac{\partial u_x}{\partial \tilde{t}} &= -\frac{h}{\rho\kappa}\frac{\partial p}{\partial \tilde{x}} \\ \frac{\partial u_y}{\partial \tilde{t}} &= -\frac{h}{\rho\kappa}\frac{\partial p}{\partial \tilde{y}} \\ \frac{\partial u_z}{\partial \tilde{t}} &= -\frac{h}{\rho\kappa}\frac{\partial p}{\partial \tilde{z}} + \frac{g\alpha h^2}{\kappa} T \end{aligned}\right\} \tag{13}$$

$$\frac{\partial T}{\partial \tilde{t}} - \frac{h^2\beta}{\kappa} u_z = \frac{\partial^2 T}{\partial \tilde{x}^2} + \frac{\partial^2 T}{\partial \tilde{y}^2} + \frac{\partial^2 T}{\partial \tilde{z}^2} \tag{14}$$

where, as is common practice, the nondimensional coordinates $(\tilde{x}, \tilde{y}, \tilde{z}) = (x/h, y/h, z/h)$ and $\tilde{t} = tk/h^2$ have been introduced, h being the depth of the liquid layer. In what follows, the symbol " $\sim$ " will always refer to a dimensionless quantity. Also, the Cartesian coordinate system with respect to the fluid is that shown in Fig. 13.

When the disturbance variables of the type of Eq. (11) are substituted into the expressions shown above, there results

$$i\tilde{l}u_x^* + i\tilde{m}u_y^* + Du_z^* = 0 \tag{15}$$

$$\left.\begin{aligned} \tilde{q}u_x^* &= -\frac{i\tilde{l}h}{\kappa\rho} p^* \\ \tilde{q}u_y^* &= -\frac{i\tilde{m}h}{\kappa\rho} p^* \\ \tilde{q}u_z^* &= -\frac{h}{\rho\kappa} Dp^* + \frac{g\alpha h^2}{\kappa} T^* \end{aligned}\right\} \tag{16}$$

$$\tilde{q}T^* - \frac{h^2\beta}{\kappa} u_z^* = (D^2 - \tilde{l}^2 - \tilde{m}^2)T^* \tag{17}$$

where D is the operator $d/d\tilde{z}$, $\tilde{q} = q\kappa/h^2$, $\tilde{l} = lh$, and $\tilde{m} = mh$. Again, an asterisk denotes the portion of the given variable that depends on $\tilde{z}$ only.

Next, by combining Eqs. (15) and (16) to eliminate u_x^*, u_y^*, and p^*, we obtain

$$\tilde{q}(D^2 - \tilde{l}^2 - \tilde{m}^2)u_z^* = -(\tilde{l}^2 + \tilde{m}^2)\frac{g\alpha h^2}{\kappa} T^* \tag{18}$$

which may be combined with Eq. (17) to yield a single equation in terms of either T^* or u_z^*,

$$\tilde{q}(D^2 - \tilde{a}^2)^2 T^* - \tilde{q}^2(D^2 - \tilde{a}^2)T^* - \frac{\tilde{a}^2 g\alpha\beta T^* h^4}{\kappa^2} = 0 \tag{19}$$

$$\tilde{q}(D^2 - \tilde{a}^2)^2 u_z^* - \tilde{q}^2(D^2 - \tilde{a}^2)u_z^* + \left(\tilde{a}^4\tilde{q} - \tilde{a}^2\frac{g\alpha\beta h^4}{\kappa^2}\right)u_z^* = 0 \tag{20}$$

where $\tilde{a}^2$ has replaced $\tilde{l}^2 + \tilde{m}^2$.

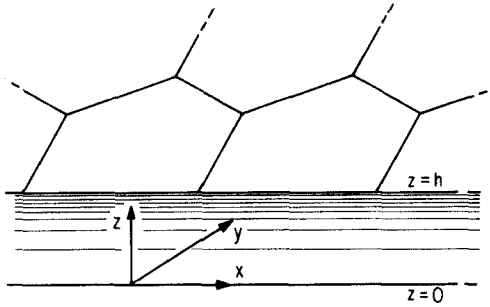

FIG. 13. Orientation of Cartesian coordinates in horizontal fluid layer.

Either equation may be considered. To locate now the marginal state, we set both the real part and the imaginary part of $\tilde{q}$ equal to zero, thus obtaining, respectively, for Eqs. (19) and (20),

$$\tilde{a}^2\left(\frac{g\alpha\beta h^4}{\kappa^2}\right)T^* = 0 \tag{21}$$

$$\tilde{a}^2\left(\frac{g\alpha\beta h^4}{\kappa^2}\right)u_z^* = 0 \tag{22}$$

It follows in this simple case that the marginal state is specified by the condition

$$\tilde{a}^2\frac{g\alpha\beta h^4}{\kappa^2} = 0 \tag{23}$$

The system is therefore stable whenever

$$\tilde{a}^2\frac{g\alpha\beta h^4}{\kappa^2} < 0 \tag{24a}$$

but unstable if

$$\tilde{a}^2\frac{g\alpha\beta h^4}{\kappa^2} > 0 \tag{24b}$$

Since all quantities on the left of Eq. (23), except for the temperature gradient β, are always positive, the sign of the expression depends on the sign of β. The conclusion which is reached on the basis of such an inviscid analysis is that a layer of fluid is always unstable when the temperature *decreases* upward ($\beta > 0$) and always stable when the temperature *increases* upward ($\beta < 0$).[4]

The stability analysis will now be extended to the more realistic case which includes the effect of viscosity. The pertinent equations are Eqs. (8)–(11); or, in nondimensional form, Eqs. (12), (14), and

$$\left.\begin{aligned} \frac{\partial u_x}{\partial \tilde{t}} &= -\frac{h}{\rho\kappa}\frac{\partial p}{\partial \tilde{x}} + N_{\mathrm{Pr}}\,\mathrm{div}(\mathrm{grad}\,u_x) \\ \frac{\partial u_y}{\partial \tilde{t}} &= -\frac{h}{\rho\kappa}\frac{\partial p}{\partial \tilde{y}} + N_{\mathrm{Pr}}\,\mathrm{div}(\mathrm{grad}\,u_y) \\ \frac{\partial u_z}{\partial \tilde{t}} &= -\frac{h}{\rho\kappa}\frac{\partial p}{\partial \tilde{z}} + \frac{g\alpha h^2}{\kappa}T + N_{\mathrm{Pr}}\,\mathrm{div}(\mathrm{grad}\,u_z) \end{aligned}\right\} \tag{25}$$

where $N_{\mathrm{Pr}} = \nu/\kappa$ is the Prandtl number. These are now solved formally by assuming that

$$\begin{aligned}(u_x, u_y, u_z, p, T) = [u_x^*(\tilde{z}), u_y^*(\tilde{z}), u_z^*(\tilde{z}), p^*(\tilde{z}), T^*(\tilde{z})] \\ \times e^{i\tilde{l}\tilde{x}}\, e^{i\tilde{m}\tilde{y}}\, e^{\tilde{q}\tilde{t}}\end{aligned} \tag{26}$$

for which Eqs. (12), (14) and (25) become (15), (17), and

$$\left.\begin{aligned} \tilde{q}u_x^* &= -\frac{i\tilde{l}h}{\kappa\rho}p^* + N_{\mathrm{Pr}}(D^2 - \tilde{a}^2)u_x^* \\ \tilde{q}u_y^* &= -\frac{i}{\rho\kappa}\frac{h}{}p^* + N_{\mathrm{Pr}}(D^2 - \tilde{a}^2)u_y^* \\ \tilde{q}u_z^* &= -\frac{h}{\rho\kappa}Dp^* + \frac{g\alpha h^2}{\kappa}T^* + N_{\mathrm{Pr}}(D^2 - \tilde{a}^2)u_z^* \end{aligned}\right\} \tag{27}$$

Eqs. (27) are next combined with Eq. (15) to yield an expression analogous to Eq. (18):

$$(D^2 - \tilde{a}^2)[N_{\mathrm{Pr}}(D^2 - \tilde{a}^2) - \tilde{q}]u_z^* - \tilde{a}^2\frac{g\alpha h^2}{\kappa}T^* = 0 \tag{28}$$

[4] In certain rare instances, such as for water between 0 and 4°C, α, the coefficient of thermal expansion of the fluid, is negative. In such instances, the converse of the stated conclusion would be true.

which, because of Eq. (17), becomes

$$(D^2 - \tilde{a}^2 - \tilde{q})(D^2 - \tilde{a}^2 - \tilde{q}/N_{\mathrm{Pr}})(D^2 - \tilde{a}^2)T^* + \tilde{a}^2 RT^* = 0 \qquad (29)$$

or

$$(D^2 - \tilde{a}^2 - \tilde{q})(D^2 - \tilde{a}^2 - \tilde{q}/N_{\mathrm{Pr}})(D^2 - \tilde{a}^2)u_z^* + \tilde{a}^2 Ru_z^* = 0 \qquad (30)$$

where $R \equiv g\alpha\beta h^4/\kappa\nu$ is the Rayleigh number.[5]

Either Eq. (29) or Eq. (30) may be considered as the governing equation, subject to the appropriate boundary conditions of which six are required, three at the bottom surface ($\tilde{z} = 0$) and three at the top ($\tilde{z} = 1$). These boundary conditions may be expressed in terms of either T^* or u_z^*. Rayleigh considered the case in which both surfaces were isothermal, rigid, and "free,"

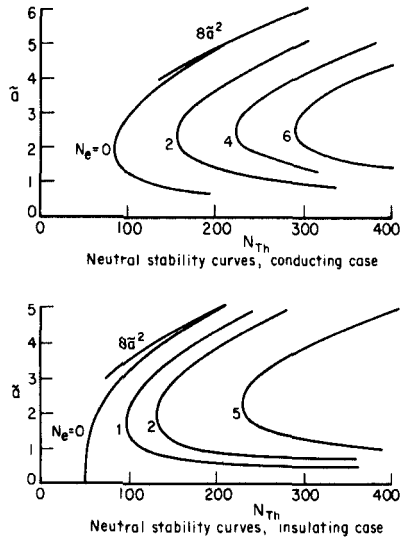

FIG. 14. Neutral stability curves as computed by Pearson.

and although the latter was an unrealistic condition, it simplified the problem to the point of allowing an analytic solution.

Invoking now the principle of exchange of stabilities, we seek to locate the stationary marginal state by setting both the real and the imaginary parts of $\tilde{q}$ equal to zero, so that Eqs. (29) and (30) become

$$(D^2 - \tilde{a}^2)^3 T^* + \tilde{a}^2 RT^* = 0 \qquad (31)$$

$$(D^2 - \tilde{a}^2)^3 u_z^* + \tilde{a}^2 Ru_z^* = 0 \qquad (32)$$

[5] The Rayleigh number is seen to be the product of the Grashof and Prandtl numbers used in empirical studies of free-convection systems.

which must be solved subject to the boundary conditions shown in Table II. In particular, we seek to determine the smallest characteristic value for R in terms of the wave number $\tilde{a}$.

TABLE II

BOUNDARY CONDITIONS FOR RAYLEIGH'S PROBLEM

		In terms of temperature	In terms of velocity	Physical meaning
$\tilde{z}=1$	(i)	$\boxed{T^*=0}$	$D^4u_z^*=0$	Isothermal surface
	(ii)	$D^2T^*=0$	$\boxed{u_z^*=0}$	Rigid surface
	(iii)	$D^4T^*=0$	$\boxed{D^2u_z^*=0}$	Free slip
$\tilde{z}=0$	(iv)	$\boxed{T^*=0}$	$D^4u_z^*=0$	Isothermal surface
	(v)	$D^2T^*=0$	$\boxed{u_z^*=0}$	Rigid surface
	(vi)	$D^4T^*=0$	$\boxed{D^2u_z^*=0}$	Free slip

It can easily be shown that the general solution to Eq. (31) [or (32)] may be expressed as

$$T^* = \sum_{i=1}^{6} A_i \, e^{s_i \tilde{z}} \tag{33}$$

where the s_i's are the roots of the indicial equation

$$(s^2 - \tilde{a}^2)^3 + \tilde{a}^2 R = 0 \tag{34}$$

These are

$$s_1, s_2 = \pm i\tilde{a}(\lambda - 1)^{1/2}$$

$$s_3, s_4 = \pm \frac{\tilde{a}}{(2)^{1/2}} [(1 + \lambda + \lambda^2)^{1/2} + (1 + \tfrac{1}{2}\lambda)]^{1/2} + i[(1 + \lambda + \lambda^2)^{1/2} - (1 + \tfrac{1}{2}\lambda)]^{1/2}$$

$$s_5, s_6 = \pm \frac{\tilde{a}}{(2)^{1/2}} [(1 + \lambda + \lambda^2)^{1/2} + (1 + \tfrac{1}{2}\lambda)]^{1/2} - i[(1 + \lambda + \lambda^2)^{1/2} - (1 + \tfrac{1}{2}\lambda)]^{1/2}$$

where $\lambda = (R/\tilde{a}^4)^{1/3}$.

In addition we require the determinant

$$\begin{vmatrix} e^{s_1} & e^{s_2} & e^{s_3} & e^{s_4} & e^{s_5} & e^{s_6} \\ s_1^2 e^{s_1} & s_2^2 e^{s_2} & s_3^2 e^{s_3} & s_4^2 e^{s_4} & s_5^2 e^{s_5} & s_6^2 e^{s_6} \\ s_1^4 e^{s_1} & s_2^4 e^{s_4} & s_3^4 e^{s_3} & s_4^4 e^{s_4} & s_5^4 e^{s_5} & s_6^4 e^{s_6} \\ 1 & 1 & 1 & 1 & 1 & 1 \\ s_1^2 & s_2^2 & s_3^2 & s_4^2 & s_5^2 & s_6^2 \\ s_1^4 & s_2^4 & s_3^4 & s_4^4 & s_5^4 & s_6^4 \end{vmatrix} = 0 \quad (35)$$

if Eq. (31) is to possess a nontrivial solution.

Rayleigh did not proceed exactly in this general way. Rather, because of the particular boundary conditions that he selected (summarized in Table II), he was able to set T^* proportional to sin $(j\pi\tilde{z})$, where j is an integer. Then, on account of Eq. (31),

$$(j^2\pi^2 + \tilde{a}^2)^3 - \tilde{a}^2 \mathrm{R} = 0 \quad (36)$$

and therefore,

$$\mathrm{R} = (j^2\pi^2 + \tilde{a}^2)^3/\tilde{a}^2$$

From this it follows that the critical Rayleigh number (or $g\alpha\beta h^4/\kappa\nu$) is $27\pi^4/4 = 657.5$, corresponding to $j = 1$ and to $\tilde{a} = \pi/2^{1/2} = 2.22$. Thus, as Bénard had observed, it is indeed possible that a layer of viscous fluid can be thoroughly stable to all infinitesimal perturbations, even when the "higher temperature is on the under side," and that convection can result only when a certain critical density gradient (temperature gradient) is exceeded.

To summarize then, Rayleigh, motivated by Bénard's experiments, deduced the conditions for the existence of stability (preconvective equilibrium) in viscous fluid layers heated from below, and laid the framework for the hydrodynamic stability analysis of such phenomena. However, as Rayleigh himself pointed out, the boundary conditions he employed corresponded neither to the experiments of Bénard, nor perhaps to any physically realizable system, and it became necessary therefore to extend Rayleigh's problem to other sets of boundary conditions.

4. *Refinements and Extensions of Rayleigh's Analysis*

Rayleigh's approach to the thermal convection problem has been extended to include other boundary conditions, the more important of which are shown in Table III. Such a refinement can be accomplished either by solving a complicated characteristic equation of the type of Eq. (35), or by resorting to a "short cut."

On purely qualitative grounds Low and Brunt (L8), in 1925, proposed that the presence of a solid wall in place of a free surface should double Rayleigh's criterion for instability and that solid walls at both top and bottom should quadruple the critical Rayleigh number.

TABLE III

SUMMARY OF BOUNDARY CONDITIONS USED IN THE RAYLEIGH PROBLEM

	Type of surface	In terms of temperature	In terms of velocity
(i)	Rigid	$(D^2 - a^2)T^* = 0$	$u_z^* = 0$
(ii)	(a) Free slip	$D^2(D^2 - a^2)T^* = 0$	$D^2u_z^* = 0$
	(b) No slip	$D(D^2 - a^2)T^* = 0$	$Du_z^* = 0$
(iii)	(a) Conducting	$T^* = 0$	$(D^2 - a^2)u_z^* = 0$
	(b) Constant flux	$DT^* = 0$	$D(D^2 - a^2)u_z^* = 0$
	(c) Radiating	$(D + K)T^* = 0$	$(D + K)(D^2 - a^2)u_z^* = 0$

In 1926–27, Jeffreys (J3, J4) attempted to extend Rayleigh's result to a more realistic set of boundary conditions, first using finite differences to obtain successive approximations to the solution of Eq. (31) and later using a method of undetermined coefficients for the case corresponding to two solid conducting boundaries. In the latter manner, he computed a critical Rayleigh number of 1709.5.

On the other hand, an earlier article of G. I. Taylor (T1) had already dealt with the stability of a viscous fluid in the annular region between a pair of coaxial cylinders rotating at different speeds, for which Taylor had shown that the initial Couette flow will break down into a series of toroidal vortices (now known as Taylor's vortices) if the relative speed of the two cylinders exceeded a certain critical value. As noted by Low (L8), this case was completely analogous to the Rayleigh problem involving two solid conducting boundaries, since the governing equations and boundary conditions for both problems are formally the same when the radii of the cylinders are nearly equal and when the cylinders are rotating at nearly the same speed. In Taylor's analysis, the "Taylor" number

$$\mathrm{Ta} = 4(\Omega h^4/\nu^2) > 0 \tag{37}$$

where Ω is the angular velocity of the cylinders, took the place of the Rayleigh number and its value at the critical point was found to equal 1706, corresponding to $\tilde{a} = \pi$. In addition Taylor accompanied his theory with a set of careful experiments, which dramatically verified his numerical predictions with respect to both the critical Taylor number and the vortex size and

thus provided the first unquestionable success for the linear stability analysis of a viscous fluid. Expecting to find a critical R around 1706, Low undertook to solve, the Rayleigh problem for solid boundaries (L6), and arrived at a critical R of 1704.4 for the case of two solid conducting boundaries. More important, he also obtained a critical R of 1108 for the case of a solid conducting boundary below and a rigid but free surface above. This, together with many other results arrived at subsequently, is shown in Table IV.

TABLE IV

THE CRITICAL RAYLEIGH NUMBER AS CALCULATED BY VARIOUS INVESTIGATORS FOR DIFFERENT BOUNDARY CONDITIONS

Type of boundary conditions[a]	Solved by	Critical R
Free-free	Rayleigh (R4), 1916	657.5
Solid-solid	Jeffreys (J1), 1928	1709.5
	Low (L6), 1929	1704.4
	Pellew and Southwell (P3), 1940	1707.8
Solid-free	Low (L6), 1929	1108
	Pellew and Southwell (P3), 1940	1100.65
Solid-solid (constant flux; top)	Sparrow *et al.* (S11), 1964	1295.781
Solid-solid (constant flux; top and bottom)	Sparrow *et al.* (S11), 1964	720.000
Solid-free (constant flux; top)	Sparrow *et al.* (S11), 1964	669.001
Solid-free (constant flux; top and bottom)	Sparrow *et al.* (S11), 1964	320.000

[a] All surfaces assumed rigid and isothermal unless otherwise stated.

Low also set forth the boundary conditions which would correspond to other physically real systems, noting that, in general, the bounding surfaces would not be perfect conductors and would require a thermal boundary condition of the form

$$\pm DT^* = KT^* \tag{38}$$

where K is a "radiation constant." It is worth remarking here that Eq. (38) properly describes the thermal condition at the upper surface in Bénard's experiments, and of any experiments in which the liquid layer is undergoing evaporation.

In 1940, Pellew and Southwell (P3) resolved the Rayleigh problem for "free-free," "solid-free," and "solid-solid" boundaries and obtained good

agreement with Rayleigh, Jeffreys, and Low (see Table IV). Moreover, with regard to cell shape, they freed themselves of the restriction to the rectangular configurations which had been imposed by Rayleigh and Jeffreys, writing:

> "Within the assumptions of the approximate theory... a particular size is associated with every shape of cell (such that $\tilde{a}^2$ takes a preferred value), but no particular shape is more likely than another to occur in a layer of indefinite extent. The explanation of the apparent preference for a hexagonal cell pattern must presumably be sought in a theory which takes account of second-order terms. This conjecture if correct goes some way towards explaining the rather indefinite nature of observed cell-formations" (P3).

As noted above, these authors also proved the general validity, for the Rayleigh problem, of the principle of exchange of stabilities. Further, by formulating the problem in terms of a variational principle, Pellew and Southwell devised a technique which led to a very rapid and accurate approximation for the critical Rayleigh number. Later, a second variational principle was presented by Chandrasekhar (C3). A review by Reid and Harris (R2) also includes other approximate methods for handling the "Bénard problem" with solid boundaries.

In a recent paper, Sparrow, Goldstein, and Jonsson (S11) presented the solution to the Rayleigh problem with a "radiation" boundary condition of the type of Eq. (38) at the upper free surface. Some of their results, for both a constant flux and a constant temperature bottom, are shown in Table IV. Of special interest is their solution for the limiting case of a constant-flux upper surface and a constant-flux bottom, for which the critical Rayleigh number was found to be only 320.

B. Subsequent Development

1. *Comparison of Experiment and Theory*

For historical reasons, we now compare the theory, as outlined above, with experimental observations. It was just such a comparison that led to much better understanding of the phenomenon under discussion and thus to substantial improvement in the general theoretical approach. This section will concern itself only with the *criterion of instability*; discussion of the morphology of the convection pattern will be deferred to a later point. It is advantageous now to subdivide the stability experiments into two categories: (*1*) fluid layers confined between solid plates, and (*2*) liquid layers having a single free surface. Obviously, evaporative convection belongs to this second category.

So far, all the experiments falling in the first category have been performed with both solid surfaces being maintained at constant uniform temperatures, this being in accord with boundary conditions (i)a, (ii)b, and (iii)a of Table III.

For such systems bounded by solid surfaces there has been good agreement between experiment and theory. A striking confirmation was achieved in 1935 by Schmidt and Milverton (S4), who studied the stability of a water layer confined between horizontal metal plates spaced from 4 to 5.5 mm apart, measuring the rate of heat transfer across the liquid layer as a function of temperature difference between the two plates. As described earlier, these authors noted an abrupt change in the heat-transfer coefficient at a Rayleigh number of 1770 ± 140, which compares favorably with the theoretical value of 1709. These results were further confirmed using a direct-shadow optical technique.

In 1936, Avsec (A2) confirmed Rayleigh's theory in a rough way for air layers confined between metal plates spaced from 1.1 to 6.3 cm apart. The onset of convection was detected visually by means of smoke within the chamber. In 1938, Schmidt and Saunders (S5) repeated the experiments of Schmidt and Milverton, using air as well as water, and obtained an average critical R of 1750. In 1958, an extensive study by Silveston (S9) using the Schmidt–Milverton technique confirmed the Rayleigh theory for four liquids in addition to water, for depths from 1.45 to 13 mm. Silveston's results yielded a critical Rayleigh number of 1700 ± 51.

In 1938, Chandra (C1) performed experiments with smoky air which confirmed the Rayleigh theory for depths above 1.0 cm (he employed depths from 4 mm to 1.6 cm), but for depths below this he observed a "columnar convection" for Rayleigh numbers well below the predicted critical value. In 1950, Sutton (S13) repeated the experiments of Chandra with both air and carbon dioxide and confirmed, for both gases, the occurrence of a subcritical columnar convection for depths less than 8 mm. These results appear to be due merely to the anomalous flow properties of smoke-air suspensions.

In contrast, for experiments with liquid layers having a free surface, the boundary conditions have been somewhat less definite. In most of them, the solid surface could be described accurately in terms of boundary conditions (i)a, (ii)b, and (iii)a of Table III, while the upper surface could perhaps be described fairly well by means of (i)a and (ii)a; however, experimental evidence may be cited which casts doubt on the appropriateness of both of these. The general thermal boundary condition, (iii)c, of which (iii)a and b are merely limiting cases, is usually required to complete the description of the free surface.

Experiments with free surfaces have not led to such success. Thus, although Bénard did not report the specific conditions for the onset of instability in pools of liquids, sufficient data were available to indicate a serious discrepancy

with Rayleigh's theory. In particular, Low and Brunt (L10) stated in 1925 that Bénard's convection "sets in with less than one-tenth of the gradient required by theory." They blamed the disagreement partly on the unrealistic boundary conditions used by Rayleigh, but primarily on the lack of knowledge concerning the viscosity and the thermal conductivity of spermaceti. Bénard himself (in Low, L7) acknowledged the discrepancy in 1930 as being a factor of 10^{-4} or 10^{-5}, while Vernotte (V2) in 1936 estimated the ratio at roughly 10^{-2}.

Of the numerous convective experiments in horizontal liquids with free surfaces subsequent to Bénard's, only a few have yielded data that permit the calculation of a stability criterion; all these, however, show a grave discrepancy with the Rayleigh theory. In 1939, Volkovisky (V4) presented a study of convection in horizontal layers of various liquids, in which measurements of thermal conditions and layer thicknesses at the onset of instability were recorded for comparison with the Rayleigh theory. In Volkovisky's experiments, water, ethyl alcohol, and several hydrocarbon oils, were made to flow with a translational velocity of the order of a few millimeters per second, and the temperature gradients giving rise to instability were produced by heating the liquids from below. Gradients of the order of 10–500°C/cm were established. Critical Rayleigh numbers were computed from Volkovisky's data for three different liquids at depths of 1 and 2 mm, as follows:

h(cm)	Water	Ethyl alcohol	Shell B14 oil[6]
0.1	32.0	38.3	5.3
0.2	131.5	194.6	34.3

These results indicate a discrepancy ranging from 1/2 to 1/200 with predictions based on the Rayleigh theory using the most nearly appropriate boundary conditions, those of Sparrow *et al.* In addition the lack of consistency in the discrepancy suggested that in these experiments the propensity of the system to exhibit convective instability was not characterized by the Rayleigh number, but rather by other parameters indicative of a new mechanism.

In 1956, Block (B14) briefly described further experimental work on convective stability criteria in liquid pools down to thicknesses as small as 50 μ, and noted that "at that thickness there was no indication that the limiting thickness, below which there would be stability, had been reached." Block continued: "This thickness is at least an order of magnitude smaller than the predicted critical depth for convective instability." Presumably Block established the temperature gradients by heating the liquid from below, but he gave no indication of the size of these gradients.

[6] A refined, heavy, viscous hydrocarbon oil. Volkovisky reports viscosity data but no other physical properties. The critical Rayleigh number, however, is reported.

Observations of Bénard patterns in drying paint films by Bell in 1952 [(B3); cf. Fig. 18b, p. 106] as well as by others (L7) indicated that convection could occur even when the Rayleigh number was negative, since these patterns occurred even when the free surface was made the under side.

Experimental information concerning the criteria for the onset of *evaporative* convection was reported in 1961 by Spangenberg and Rowland (S10), by Jarvis (J2), and more recently by Berg (unpublished). Spangenberg and Rowland studied evaporative convection in "deep" pools of evaporating water. No convection was observed for thicknesses less than 1 cm; for greater thicknesses evaporation times of approximately 70 sec were required to establish temperature gradients sufficient to cause instability. The Rayleigh number corresponding to the onset of convection was 1193, computed by "summing the R derived for each of several elementary strips, using the local temperature gradient indicated by the data." Temperature differences within the fluids were measured with a thermopile.

Jarvis' experiments (J1), in which he measured the surface temperature of evaporating water with a thermistor probe, suggested that the critical *depth* for the onset of evaporative convection in water at room temperature was 4 mm, but temperature profiles corresponding to conditions at the onset of evaporative convection were not reported. As described earlier, the presence or absence of evaporative convection was determined by the presence or absence of rapid temperature fluctuations near the surface.

Recently, Berg (B12a) obtained order-of-magnitude Rayleigh numbers for the onset of evaporative convection in 1-mm deep layers of six pure liquids, as shown in Table A. In these runs the onset of convection was detected with

TABLE A

Liquid	R_c
Acetone	300
Benzene	75
Carbon tetrachloride	100
n-Heptane	60
Isopropyl alcohol	30
Methyl alcohol	60

a schlieren system, and the corresponding temperature profiles (which were nearly linear) were determined from cross plots of temperature-time curves obtained with a thermocouple probe.

A new type of discrepancy was uncovered by Jeffreys (J5) who showed in 1951 that, in contrast to the observations of Bénard, buoyancy-driven convection must lead to a free liquid surface that is *convex* over centers of ascending warm liquid.

The failure to obtain experimental confirmation of the Rayleigh theory when a free liquid surface is involved suggests that the Rayleigh theory based on the buoyancy mechanism is not adequate for such liquid systems. This is indeed the case; for, as had been known since the initial observations of Thompson in 1855, the liquid surface itself is the seat of the potential energy required to set the bulk fluid into motion. That the gradient of surface potential energy (i.e., of surface tension) established by temperature differences along the surface provides sufficient force to set a liquid layer in motion was confirmed quantitatively by Volkovisky (V3) in 1935, and by Luntz (L9) who in 1937 studied the flow of a liquid film ("festoon vortices") up a solid surface cooler above than below. Loewenthal (L5) had confirmed this effect as it is produced by concentration differences in 1931. Finally, Bénard himself had regarded surface tension as responsible for the free surface being concave above the centers of ascension of warm liquid when he remarked, "Surface tension, acting alone, produces a depression in the center of the cells, and an excess of static pressure along the boundary lines separating the concave depressions." In a sense, he also considered the possibility that the surface tension gradients could provide the driving force for the cellular convection itself.

2. *Pearson's Theory; the Surface Tension Mechanism*

The work of Bell, Block, and others motivated J. R. A. Pearson (P2) to propose in 1958 a radically different theoretical model for the thermal convection problem: a constant density layer with temperature-dependent surface tension.

In Pearson's analysis, the fluid is assumed to be supporting an adverse linear[7] temperature gradient β, and all the fluid properties except for the surface tension σ are taken to be independent of temperature. Thus, the governing equations for the present system are identical to those of the Rayleigh problem, except for the absence of the gravitational term, so that, in place of Eq. (29), there results

$$(D^2 - \tilde{a}^2)(D^2 - \tilde{a}^2 - \tilde{q})[\mathrm{Pr}(D^2 - \tilde{a}^2) - \tilde{q}]T^* = 0 \tag{39a}$$

which simplifies to

$$(D^2 - \tilde{a}^2)^3 T^* = 0 \tag{39b}$$

if, as was verified recently (V5), the principle of exchange of stabilities is assumed to hold.

[7] The use of a linear profile, even for systems where the profiles are not linear, has been justified somewhat by Batchelor (B1), who showed that the most unstable case for any given temperature drop across the layer occurs when the gradient β is replaced by its maximum value.

Pearson's boundary conditions are shown in Table V. Equation (i) represents a heat balance at the upper surface where heat lost at a rate proportional to the surface temperature (such as by evaporation) is balanced by heat conducted to the surface from the liquid beneath. For the thermal conditions at the lower surface, two cases are considered as shown in Eqs. (iv): the surface is assumed either to be isothermal ($T^* = 0$) or to support a constant heat flux ($DT^* = 0$). Equations (ii) and (v) follow from the assumed nondeformability

TABLE V

BOUNDARY CONDITIONS FOR PEARSON'S PROBLEM

	In terms of temperature	In terms of velocity	Physical meaning
Top surface ($\tilde{z} = 1$)	(i) $(D + N_e)T^* = 0$	$(D + N_e)(D^2 - \tilde{a}^2)u_z^* = 0 = 0$	Radiating or evaporating
	(ii) $(D^2 - \tilde{a}^2)T^* = 0$		
	(iii) $D^2(D^2 - \tilde{a}^2)T^* = \tilde{a}^2 N_{Th} T^*$		Rigid balance tangential force
Bottom surface ($\tilde{z} = 0$)	(iv) (a) $T^* = 0$	$(D^2 - \tilde{a}^2)u_z^* = 0$	Conducting
	(b) $DT^* = 0$	$D(D^2 - \tilde{a}^2)u_z^* = 0$	Constant flux
	(v) $(D^2 - \tilde{a}^2)T^* = 0$	$u_z^* = 0$	Rigid
	(vi) $D(D^2 - \tilde{a}^2)T^* = 0$	$Du_z^* = 0$	No slip

(rigid flatness) of both surfaces. Equation (iii) balances the surface forces due to the temperature-induced variation in surface tension against the shear stress of the underlying fluid, while Eq. (vi) expresses the condition of no slip at the lower surface.

The heart of Pearson's analysis lies in Eq. (iii), in which he accounts for the temperature variation in the surface tension:

$$\sigma = \sigma_0 + (\partial\sigma/\partial T_0)\hat{T}_s \tag{40}$$

Here σ is the surface tension, σ_0 is its value in the undisturbed state, and $\hat{T}_s$ is the disturbance temperature at the surface. The net surface tension force at a given point on the surface (equal to grad σ) then becomes $(\partial\sigma/\partial T_0)$ grad $\hat{T}_s$, where grad refers to the surface gradient.

The viscous traction of the underlying fluid is given by

$$\tau_z = \mathbf{e}_x \mu\left(\frac{\partial u}{\partial y} + \frac{\partial v}{\partial x}\right) + \mathbf{e}_y \mu\left(\frac{\partial w}{\partial x} + \frac{\partial u}{\partial z}\right) \tag{41}$$

where u, v, and w are the velocity components in the x, y, and z directions, respectively, and $\mathbf{e}_x$ and $\mathbf{e}_y$ are unit vectors in the x and y directions.

Equating now the surface divergences of the above two forces and dropping the superscript ^ yields

$$\mu\left[\frac{\partial}{\partial x}\left(\frac{\partial u}{\partial y}+\frac{\partial v}{\partial x}\right)+\frac{\partial}{\partial y}\left(\frac{\partial w}{\partial x}+\frac{\partial u}{\partial z}\right)\right]=\left(\frac{\partial \sigma}{\partial T_0}\right)\nabla_1{}^2 T_s \tag{42}$$

where $\nabla_1{}^2 = \partial^2/\partial x^2 + \partial^2/\partial y^2$. Upon substitution of the continuity equation and introduction of Eq. (17), Eq. (42) reduces to Eq. (iii), where we have chosen to term the dimensionless group

$$\left[\frac{-\beta h^2(d\sigma/dT)}{\mu\kappa}\right] \equiv N_{\mathrm{Th}}$$

the Thompson number,[8] after James Thompson who was the first to explain surface tension driven flow. Note that, since $d\sigma/dT$ is negative, N_{Th} is always positive when the liquid supports an adverse temperature gradient.

The solution to Pearson's problem may be expressed as

$$N_{\mathrm{Th}}=\frac{8\tilde{a}(\tilde{a}\cosh\tilde{a}+N_e\sinh\tilde{a})(\tilde{a}-\sinh\tilde{a}\cosh\tilde{a})}{\tilde{a}^3\cosh\tilde{a}-\sinh^3\tilde{a}} \tag{43}$$

for the conducting case, and

$$N_{\mathrm{Th}}=\frac{8\tilde{a}(\tilde{a}\cosh\tilde{a}+N_e\sinh\tilde{a})(\tilde{a}-\sinh\tilde{a}\cosh\tilde{a})}{(\tilde{a}^3\sinh\tilde{a}-\tilde{a}^2\cosh\tilde{a}+2\tilde{a}\sinh\tilde{a}-\sinh^2\tilde{a}\cosh\tilde{a})} \tag{44}$$

for the constant flux case.

These results are plotted in Fig. 14 (see p. 89). For $N_e = 0$, the critical Thompson number becomes 80 for the conducting case and 48 for the insulating case, which correspond to values of $\tilde{a}$ equal to 2.0 and 0, respectively.

Following Pearson, we compare now the "critical thickness" of the fluid layer as computed from the theory based on the surface tension mechanism, with that based on Rayleigh's analysis of buoyancy-driven flows. One easily obtains that, for the conducting case,[9]

$$h_c\,(\text{surface tension}) = \left[\frac{80\rho\nu\kappa}{-(d\sigma/dT)\beta}\right]^{1/2}$$

and

$$h_c\,(\text{buoyancy}) = \left[\frac{1108\nu\kappa}{g\alpha\beta}\right]^{1/4}$$

[8] This group has also been termed the Marangoni number.

[9] Actually, in Pearson's calculation, the critical Rayleigh number was taken equal to 571, the value obtained by Jeffreys using incorrect boundary conditions. The correct value, 1108, was arrived at by Low.

which will be equal for a fluid depth of

$$\bar{h}_c = \left[\frac{-(d\sigma/dT)}{\rho g \alpha} \cdot \frac{1108}{80}\right]^{1/2}$$

This led Pearson to remark:

> "For most liquids at laboratory temperatures this relation leads to values for $\bar{h}_c$ of the order of 1 cm. For thicknesses less than $\bar{h}_c$, then, we expect surface tension forces to be more effective than buoyancy forces in producing instability, and, for values of (h) as small as 1 mm, the onset of cellular motion could confidently be attributed to surface tension rather than to buoyancy" (P2).

Pearson went on to conclude that all of Bénard's experiments involved surface tension driven convection. Thus, in the case of spermaceti at 100°C, reasonable estimates for κ (5×10^{-4}) and ν (5×10^{-2}) and Bénard's reported values[10] for $-(d\sigma/dT)$ (5×10^{-2}), ρ (0.806) and α (7.7×10^{-4}), yield, for a 1-mm layer supporting a 1° temperature drop,

$$N_{\mathrm{Th}} = \frac{(0.05)(10)(0.1)^2}{(0.806)(0.05)(5 \times 10^{-4})} = 248 > 89 \qquad \text{(unstable)}$$

$$R = \frac{(980)(7.7 \times 10^{-4})(10)(0.1)^4}{(0.05)\,(5 \times 10^{-4})} = 30 < 1108 \qquad \text{(stable)}$$

Also, Volkovisky's stability data (see p. 96) can now be checked against the predictions based on Pearson's work, with the results shown in Table B.

TABLE B

h(cm)	Water		Ethyl alcohol		Shell B14	
	R	N_{Th}	R	N_{Th}	R	N_{Th}
0.1	32.0	4000	40	540	5	320
0.2	130	4000	200	920	35	510

The values for Thompson number clearly indicate instability, although there is still a considerable spread between theory and experiment. The same was also true in Berg's (B12a) experiments for which approximate critical Thompson numbers are shown in Table C. Likewise, in the experiments of Spangenberg and Rowland (with evaporative convection in water) the Thompson

[10] All these numerical quantities are reported in cgs units.

number was computed to be around 1500, also well into the unstable range.

Thus, even though it appears that the Pearson analysis is indeed the appropriate one for describing convection within thin liquid layers with a free surface, indications are that refinements in both the theory and the experiments will be required before a quantitative agreement can be achieved.

TABLE C

APPROXIMATE EXPERIMENTAL CRITICAL THOMPSON NUMBERS FOR EVAPORATION CONVECTION IN 1-MM DEEP LAYERS OF EVAPORATING LIQUIDS (B12a)

Liquid	Th
Acetone	3400
Benzene	950
Carbon tetrachloride	1400
n-Heptane	700
Isopropyl alcohol	200
Methyl alcohol	650

Pearson's assumption of free surface nondeformability has been relaxed in a recent paper by Scriven and Sternling (S7) in which the model used was that of a Newtonian fluid surface subject to infinitesimal displacements from its mean plane. It was found that, for liquid layers of the order of 1 mm deep, the neutral stability curve was affected only at very small values of $\tilde{a}$ (corresponding to disturbance wavelengths in excess of approximately 30 times the liquid depth); here N_{Th} approached minus infinity, thus implying that the system would always be unstable with respect to disturbances of very large wavelengths. Furthermore, these authors showed, in accord with the observations of Bénard, that the surface would be depressed at the cell centers where warm fluid ascends, and be elevated along the cell partitions. Since this effect is opposite to that in buoyancy-driven convection (J5), it appears that one should be able to determine experimentally whether buoyancy or surface tension dominates convection in any given situation by measuring the surface relief with any of the techniques outlined earlier.

It should be noted carefully that Pearson's analysis still contains the *assumption* that instability sets in only by a stationary marginal state, which of course excludes the actual possibility of an oscillatory marginal regime.

3. *The Combined Effect of Buoyancy and Surface Tension*

In the usual case, evaporation from the free surface of a horizontal liquid layer produces a situation favorable to both the buoyancy and the surface

tension mechanisms for evaporative convection. The distinction between them actually belongs as much to history as it does to nature, and, in a recent paper by Nield (N1), the rival mechanisms have been combined into a single analysis. The principle of exchange of stabilities was once again invoked, so that the governing equation became Eq. (31) or Eq. (32) (from the Rayleigh problem), while the boundary conditions were those of Pearson.

The numerical results for this combined problem indicate "that the two agencies causing instability reinforce one another and are tightly coupled." Nield attributes the tightness of the coupling, which can be seen in Fig. 15,

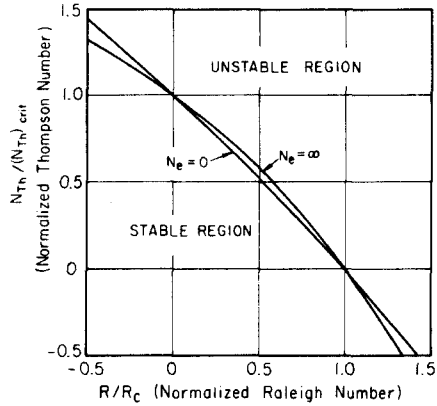

FIG. 15. Nield's stability diagram showing the combined effect of buoyancy and surface tension (N1) (courtesy of Cambridge University Press).

to the fact that cells formed by buoyancy and by surface tension are approximately of the same size.

4. *The Effect of Surface Active Agents*

As the experimental evidence concerning the stability and convective behavior of a liquid layer with a free surface was being accumulated, there arose evidence pointing to the importance of an additional factor: the presence of surface contamination. As early as 1912, Dauzère (D3) showed that a monolayer of stearic acid was capable of inhibiting the onset of convection in thin layers of melted wax. Low (L7), and later Bell (B3), demonstrated that certain silicone monolayers prevented the occurrence of Bénard cells in drying paint films, while Langmuir and Langmuir (L1) noted that monolayers of several surfactants (oleic acid, cetyl alcohol, and others) eliminated the convection normally accompanying evaporation of aqueous ether solutions. Finally, Block (B14) noted the dramatic stabilizing effect of surface films on thin layers of several organic liquids, as well as on water:

"...Wherever and as soon as the layer [of spreading silicone] passed over the Bénard cell, the surface deformation disappeared and the flow stopped. . . Then the thickness of the liquid (covered by a monofilm) was increased until cellular surface deformations and circulation could again be seen. The thickness at which this occurred was 2 mm, which is, in this case, about the critical depth for the onset of convective instability."

The observed stabilizing effect of surfactants toward convection induced by surface tension has been confirmed theoretically in a recent paper by Berg and Acrivos (B13), in which the stability analysis technique and the physical model were the same as Pearson's except that the free-surface boundary condition [(iii) of Table III] took into account the presence of surface active agents. Critical values for the Thompson number were computed as functions of two dimensionless parameters, one embodying the "surface viscosity" and the other the "surface elasticity."

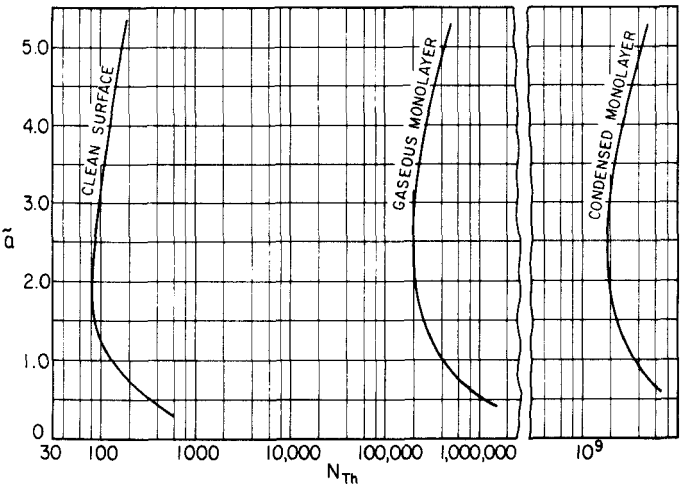

FIG. 16. Neutral stability curves showing the effect of surfactants.

The stabilizing influence of the surface viscosity of a typical monolayer was found to be negligible, in contrast to that of the "surface elasticity," which (even for a so-called "gaseous" monolayer) was sufficient to cause a dramatic stabilization. The shift in the Pearson neutral-stability curves brought about by the presence of a "gaseous" monolayer and also by a close-packed monolayer on a 1-mm deep water substrate is shown in Fig. 16. For this example, the gaseous monolayer having a surface pressure of 0.2 dyn/cm effected a 500-fold increase in the stability criterion, whereas, in

the presence of the close-packed monolayer, of stearic acid the theory predicted virtually complete elimination of the surface tension mechanism for instability.

Surface elasticity is not a structural property of the monolayer, but arises from the dependence of surface tension on the superficial concentration of the surfactant. Figure 17 depicts a small disturbance in which fluid is swept

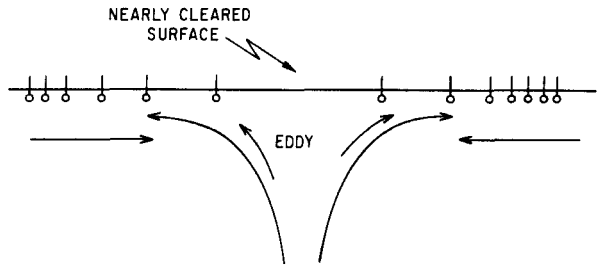

FIG. 17. Eddy bringing fresh liquid to the surface opposed by back-spreading pressure of surfactant film.

radially outward from a particular location on the surface, a disturbance which may be self-amplifying. If surfactant molecules are present, they will be swept outward with the movement of the substrate; since a local drop in surfactant concentration *increases* the surface tension, this will cause surface forces to develop which oppose the outward flow of the liquid. Such behavior simulates "elasticity."

One might have hoped that, following the modifications to the stability analyses for liquids with free surfaces, quantitative comparisons between experiment and theory could have been made, but such is not the case. Further refinement in both theory and experiment is still required. Nevertheless it is indeed encouraging that all of the experimentally observed *qualitative* effects regarding convective stability appear to be in agreement with the predictions of hydrodynamic stability theory.

IV. The Morphology of Natural Convection in Horizontal Liquid Layers

Up until this point, with the exception of the description of Bénard's results, we have concerned ourselves only with the stability criteria. Linear stability theory provided the theoretical tools, while optical and thermal methods were employed to detect experimentally the onset of instability. Quantitative agreement between experiment and theory has thus been achieved for gases and for liquids confined between solid plates, and qualitative agreement for liquids with free surfaces.

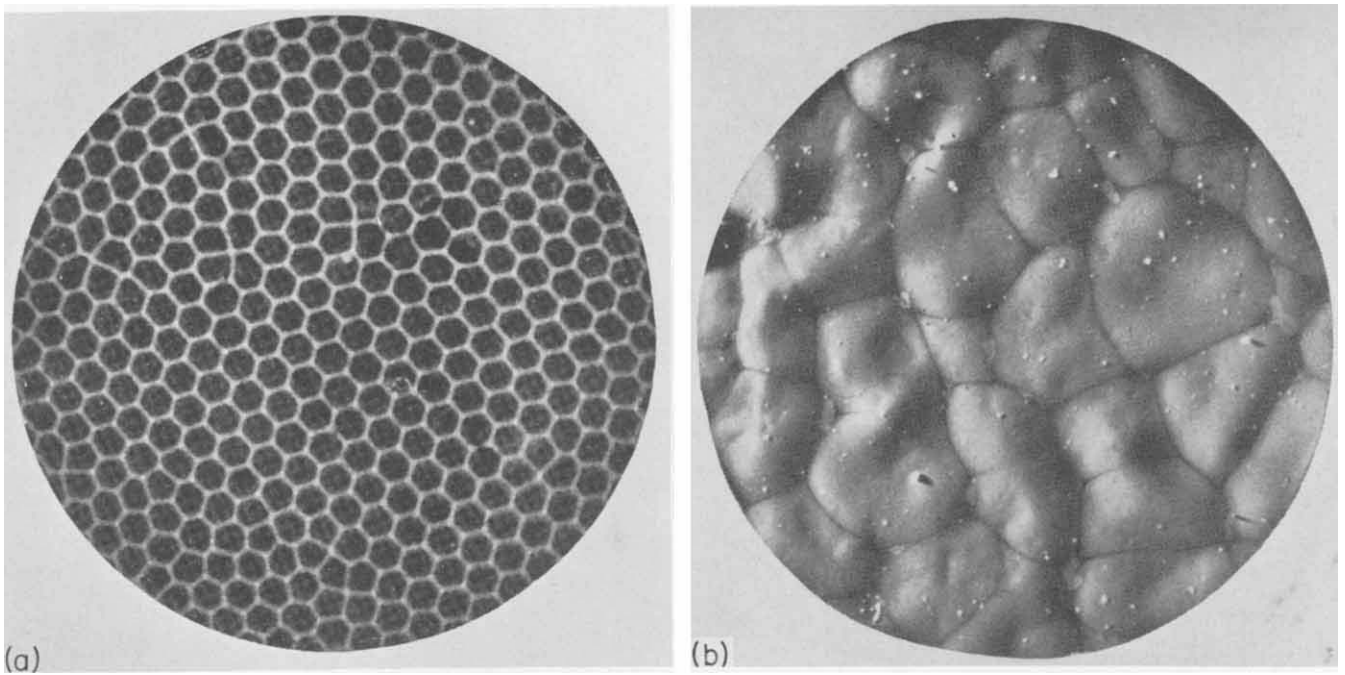

FIG. 18. (a) Bénard cells visualized by the direct-shadow method in which cell partitions act as cylindrical mirrors (A4) (see Fig. 12). Magnification 2×. (Courtesy of Ministry of Air, Paris.) (b) Bénard cells in a drying paint film (B3). Magnification about 5×. (Courtesy Oil and Colour Chemical Association, London.)

But what is known concerning the morphology of the convection? Most of the effort in this area has been experimental, and Bénard's work furnishes the foundation. He established that when a shallow liquid layer is freed of the influence of lateral walls, is subjected to no external shear, and is uniformly heated below, a regularized cellular convection pattern sets in, in which the cell divisions bear a definite relation to the thickness of the fluid layer. A photograph from Bénard's work is shown in Fig. 18, together with a photograph by Bell (B3) showing Bénard cells in a drying paint film.

We now review the more important experimental investigations following Bénard's, paying particular attention to studies of convection in liquid layers.

A. Experimental Studies

Dauzère (D1) produced solidified Bénard cells in 1907 by quickly cooling a thin layer of melted beeswax undergoing convection. Performing similar experiments in 1912 (D3, D4), he noticed that if the beeswax was boiled with water beforehand, or better still with an alkaline solution, the entire character of the cells would change. The cells isolated themselves into colonies separated by relatively quiet areas, and these colonies were eventually reduced to single isolated vortices (tourbillons isolés) (see Fig. 19) which, after 30 to 45 min,

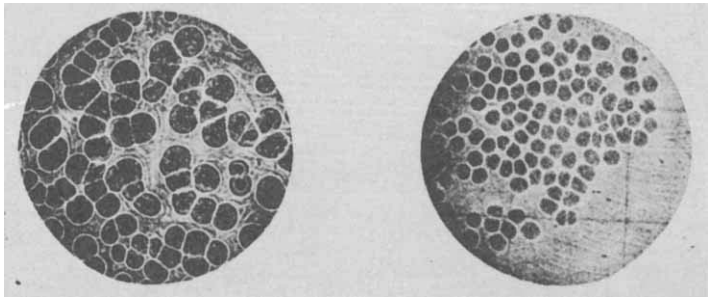

FIG. 19. Isolated Bénard cells in melted wax covered with a film of stearic acid (D5). Actual size. (Courtesy of Ministry of Air, Paris.)

would die out altogether. Dauzère first attributed the new cell species to the effect of superficial contaminants on the surface tension, but later (D5) thought that the reduced (or eliminated) circulation in the area separating the isolated vortices was due to a cohesive membrane of contaminants which tended to thermally isolate the liquid beneath it from the air above, thus reducing the heat flux and hence the convection. Unaware that the effect might be hydrodynamic instead of thermal, Dauzère cited as proof the fact that glass placed over the surface would also alter or stop the convection. Actually, in either case he had altered the "free slip" character of the liquid surface.

Dauzère later noted (D6) that if a film-covered surface was heated with sufficient intensity, yet another species of "cell" was born, often coexisting with the "isolated vortices." The pattern is worm-like in appearance (Fig. 20)

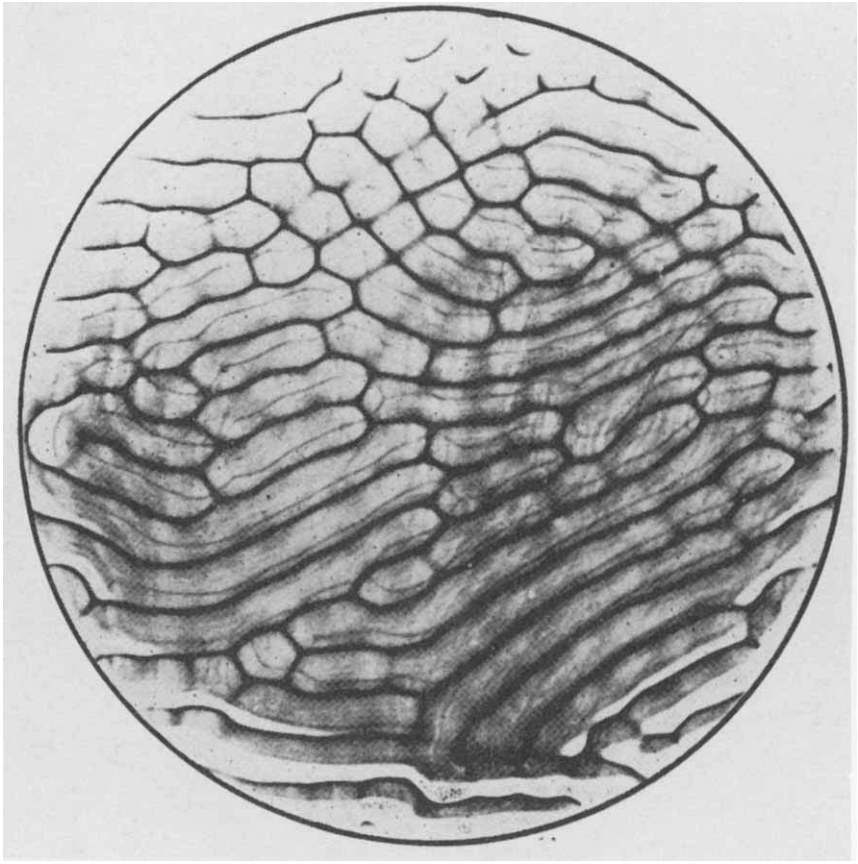

FIG. 20. Vermiculated rolls in melted wax covered with a film of stearic acid (A4). Magnification about 2×. (Courtesy of Ministry of Air, Paris.)

and Avsec (A4) later termed it one of "vermiculated rolls." This pattern bore resemblance to those produced earlier by Guebhard (cf. B6) and later by Bénard (B10) on exposed photographic plates acting as the top to a layer of photographic developer solution. Avsec (A4) observed this pattern in smoky air layers bounded on top by a glass plate. He attributed the pattern to the presence of a no-slip surface under conditions of insufficient heat flux to produce fully developed polygonal cells. Vermiculated rolls have also been observed by other investigators under other conditions, but in accord with Avsec, they have apparently always been formed at a no-slip surface.

Another type of cell pattern is formed when thin layers of some very volatile liquids evaporate. Bénard (B9) photographed an evaporating layer of ethyl ether (b.p., 35°C) and produced a permanently unsteady, roughly cellular structure. Thompson (T4), in 1882, had observed still another convective structure, which he termed "tesselations," in a deep layer of evaporating water (Fig. 1b) rendered visible by a soap scum at the surface. Thompson's "tesselations" differed from the cellular structure in a thin layer of evaporating ether in that the "cells" (i.e., the tesselations) were not closed nor did they appear to have any centers. Rather, these tesselations formed a permanently unsteady pattern as did the evaporating ether, but the motion was much more sluggish. In 1961, Spangenberg and Rowland (S10) photographed these tesselations in evaporating water by means of schlieren photography.

In 1927, the Langmuirs (L1) observed still another type of convection when they studied the evaporation of aqueous ether solutions. The convection was so violent and chaotic that the liquid surface "twitched" visibly during the evaporation.

All the experiments mentioned above seem to indicate that the size of the isolated vortices, the vermiculated rolls, and the unsteady cells (as in evaporating ether) are generally roughly proportional to the liquid depth, but no quantitative studies have ever been made on this point. In contrast, the size of the tesselations in deep water layers seems to bear no relation to depth, thus suggesting that once a given depth is exceeded the depth itself is no longer a significant parameter of the convection.

When the liquid heated below is subjected to an external shear, as in the case of a liquid flowing over a flat plate, the convection pattern usually orients itself in the direction of the shear. This was demonstrated first by Bénard (B8) (see Fig. 4) but was actually studied first by Idrac (cf. A4) in air. Later Terada (T2) investigated the phenomenon in liquids which were caused to flow down a heated flat plate. Bénard (B8, B9) compared the width of such rolls with the width predicted from Rayleigh's theory[11] obtaining a remarkable agreement which we now know was illusory. Longitudinal rolls in liquids were studied extensively by Volkovisky (V4) in 1939. He determined that at moderate flow velocities (< 3 or 4 mm/sec) and high viscosities (> 20 centistokes) the ratio of the roll width to the liquid depth was constant, between 1.90 and 2.10 for depths between 0.5 and 3.5 mm, while, for higher velocities and lower viscosities, the roll width became larger in relation to the liquid depth. When the velocity V (the overall flow velocity) was increased to 5.0 cm/sec for alcohol ($\nu^{50} = 0.9$ centistokes) and to 3.5 cm/sec for a viscous oil ($\nu^{75} = 45$ centistokes) the bands became crosshatched, forming a network of rectangular cells. Volkovisky also demonstrated the coexistence of cellular and roll vortices.

[11] This agreement was also achieved between the experimental hexagonal cell size and the size predicted by Rayleigh.

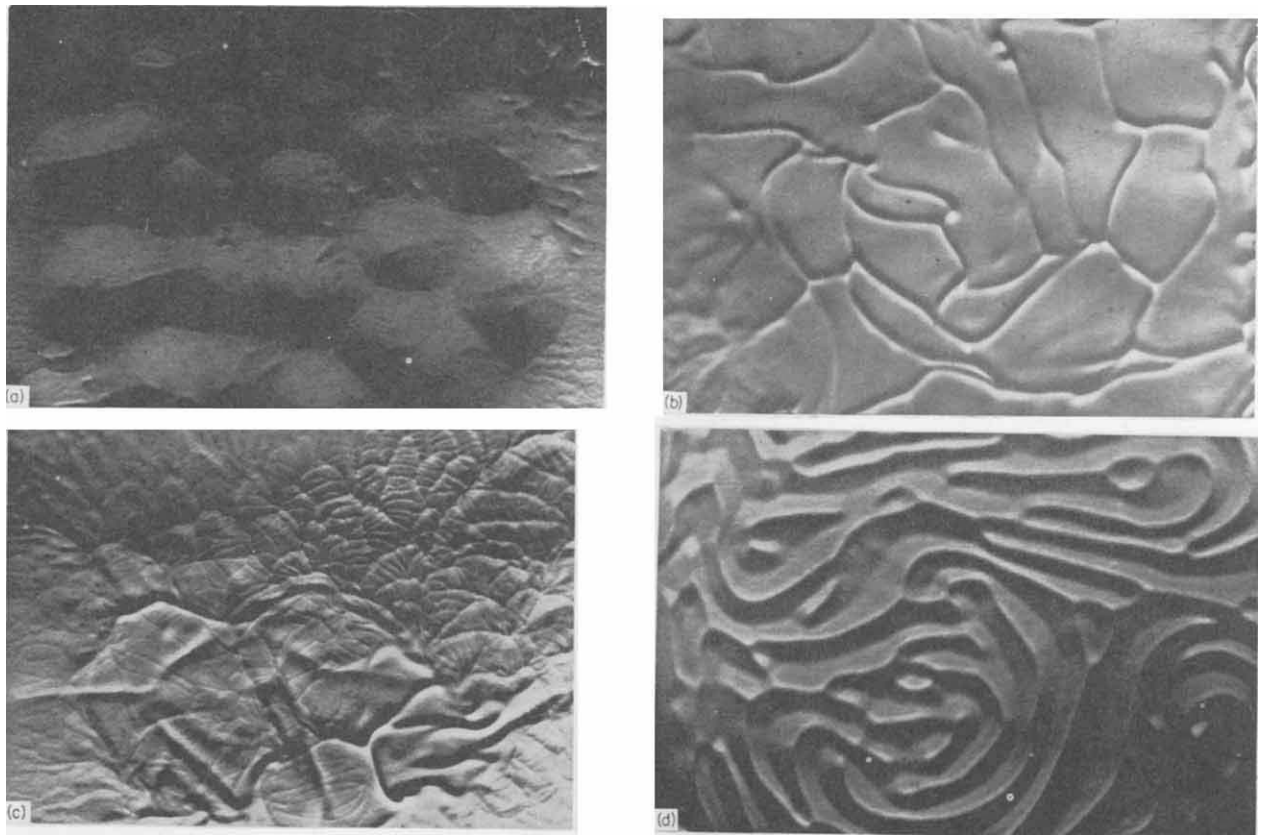

FIG. 21. Schlieren photographs of flow patterns of evaporative convection (top views, magnification 1.8×): (a) cells: methanol, $h = 2$ mm; (b) streamers: benzene, $h = 10$ mm; (c) ribs: benzene, $h = 10$ mm; (d) vermiculated rolls: carbon tetrachloride, $h = 3$ mm.

In 1938, Avsec (A3) discovered yet another vortex structure due to shear velocity, a structure showing rolls *perpendicular* to *V*. Avsec demonstrated the existence of these "bandes transversales" in air with smoke, and their discovery suggested the thermoconvective origin of cloud formations which often show bands of clouds perpendicular to the wind velocity. Avsec later published (A4) an exhaustive study of the morphology of convection in air layers and of its application to meteorology.

Using schlieren optics, Berg (B12) obtained a variety of patterns of evaporative convection in pure liquids. Studies were made with acetone, benzene, carbon tetrachloride, *n*-heptane, isopropyl alcohol, and methyl alcohol, and experiments were performed to obtain information concerning the structure of the evaporative convection pattern as it was affected by the fluid properties, the thickness of the fluid layer, the vapor phase resistance to evaporation, and the presence of surfactants.

Four principal patterns of convection were distinguished when pure liquids were employed: cells, streamers, ribs, and vermiculated rolls. These names were chosen in an attempt to describe the actual appearance of the convection patterns and in accordance with historical designations. Examples are shown in Fig. 21. The patterns depicted there were exhibited in all of the liquids under various conditions. In particular, cells appeared to be the dominant patterns in all liquids for depths of 2 mm or less, and the cell size for the various liquids at the 1-mm and 2-mm depths is shown in Table VI. For a thin (< 2 mm) layer of given liquid evaporating into still air, the cell size increased with the depth of the liquid layer, and the flow which the cellular schlieren pattern represented was the same as that observed by Bénard (see Fig. 3). These cells were quite immobile and generally neither grew nor decayed in size with time. A direct stream of dry nitrogen onto the surface of the liquid "sharpened" the cell peripheries and tended to reduce the cell size.

The second type of flow, generally observable when the liquid depth exceeded 7 or 8 mm, was that of streamers. These were "cold lines" in which cooled liquid would plunge in sheets into the interior of the fluid, as illustrated in Fig. 22. These streamers moved sluggishly about the fluid and resembled closely the networks described by Thompson, and photographed by Spangenberg and Rowland.

The third pattern, ribs, often coexisted with that of streamers when the liquid was *completely devoid* of surface contamination. These ribs moved rapidly about among the streamers, traveled perpendicular to themselves, and could be either perpendicular or parallel to the streamers. As the depth of the fluid layer was increased, ribs often began to appear even if the principal pattern was still cellular. These ribs then persisted while the depth was increased still further, with the pattern evolving into one of the streamers interspersed with these fast-moving ribs.

TABLE VI

CELL SIZE IN EVAPORATIVE CONVECTION (B12)

Material	Depth of layer (mm)	Cell width (mm)	Cell width/ layer depth
Acetone	1	8.5	8.5
	2	14.0	7.0
Benzene	1	2.8	2.8
	2	6.2	3.1
	3	15.0	5.0
	4	25.0	6.2
Carbon tetrachloride	0.25	0.8	3.2
	0.5	1.6	3.2
	1.0	5.4	5.4
	2.0	14.0	7.0
	3.0	24.0	8.0
n-Heptane	1.0	3.0	3.0
	2.0	11.0	5.5
	3.0	17.0	5.7
Isopropyl alcohol	1.0	1.7	1.7
	2.0	3.8	1.9
Methyl alcohol	1.0	4.5	4.5
	2.0	12.0	6.0
	3.0	17.0	5.6

The fourth basic convection pattern, vermiculated rolls, was associated with the *presence* of a nonvolatile material of large molecular size in the surface region. For liquids containing such a material, a vermiculated roll pattern was found to prevail at intermediate depths (3–6 mm). At depths

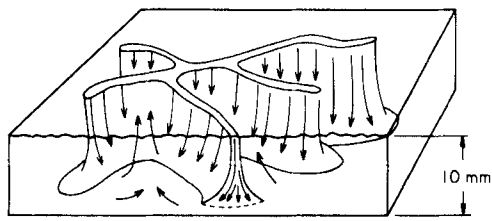

FIG. 22. Evaporative convection in cold streamers: cold fluid plunges along distinct lines in the surface and warm fluid rises slowly in the area between the streamers (B12).

of 2 and 3 mm, film-covered layers of acetone, benzene, and carbon tetrachloride all showed a pattern of vermiculated rolls while their clean-surfaced counterparts exhibited cellular convection. Figure 21(d) shows hot and cold lines side by side and wrapped around one another to give the appearance of worms, and the flow is shown diagrammatically in Fig. 23. This structure was

stable to a stream of dry nitrogen directed over the surface. Moreover, as the depth of the liquid was increased, the rolls became wider and the cold lines more distinct, while the hot lines, which originally alternated with the cold lines, became less and less well defined until they faded away altogether leaving a random network of cold lines which have been called streamers.

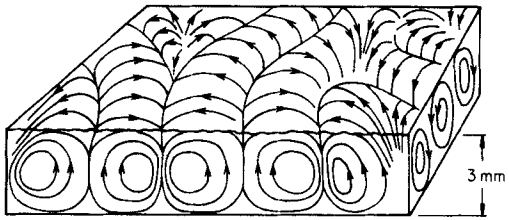

FIG. 23. Evaporative convection in vermiculated rolls: Cold fluid flows down in a relatively narrow region near the roll partition while warm fluid rises over a wider, less distinct region. As fluid depth is increased the warm partitions will lose their identity, and the cold partitions will become streamers (B12).

In summary, it has been demonstrated experimentally that during evaporation several types of convection patterns can exist in quiet shallow pools of liquids, in addition to the regular hexagons observed by Bénard; the appearance of these flow patterns can be altered drastically by the addition of surface-contaminating molecules.

B. Surface Deformations

As described earlier, Bénard performed a number of careful interferometric measurements of the deformation of the liquid surface during convection, and correctly attributed the observed relief to the forces of surface tension. Bénard's hexagonal cells were concave and were divided by ridges, whose level was 1.7 μ above the cell center when the layer of spermaceti was 1.20 mm thick and at a temperature of 100°C. Smaller thicknesses and lower temperatures yielded less pronounced ridges. Bénard's thermal measurements placed the lateral temperature difference between the cell center and the cell partitions at approximately 1°C. In 1939, Hershey (H1) obtained an expression for the steady-state surface elevation due to surface tension differences caused by temperature differences on the surface. This expression reduces to

$$\Delta h = \frac{3\,\Delta\sigma}{\rho g h} = \frac{3(d\sigma/dT)\,\Delta T_{\text{lat}}}{\rho g h} \tag{45}$$

where Δh is the difference in surface elevation and ΔT_{lat} the corresponding difference in surface temperature. Equation (45) yields a surface elevation of 1.58 μ for a 1.2-mm layer of spermaceti at 100°C with a lateral temperature

difference of 1°C. This result is in good accord with Bénard's measurements, but the dependence of the elevation on layer depth is the reverse of that indicated by Bénard. Hershey observed the surface deformations which he described by holding a glass rod, cooled in liquid air, to the bottom surface of a glass plate covered with a thin layer of liquid. While no actual measurements were taken, Hershey made the interesting observation that small amounts of surface-active agents (on water) caused the surface to flatten out completely.

It has already been mentioned that, if the surface deformation is due to buoyancy-driven thermal convection alone, the surface must be convex at the cell centers. Such behavior was observed by Spangenberg and Rowland (S10) for deep layers of evaporating water. Furthermore, in a repetition of one of Bénard's experiments, i.e., using approximately 1-mm-thick layers of melted wax, these authors obtained the puzzling result that in these systems the elevation also occurred above the cell centers.

By neglecting inertia terms, Orchard (O1) analyzed recently the two-dimensional flow of thin layers of viscous liquids and gels and obtained an expression for the rate of decay of surface irregularities. In Orchard's work, surface-tension forces varied from point to point as a result of the non-uniformity of the surface curvature.

C. Cell-Size Predictions from Linear Stability Theory

Theoretical work on the morphology of convection has been concerned chiefly with the prediction of the type and dimensions of the observed "cells" in terms of the liquid depth, the fluid properties, and the temperature difference between the top and bottom (or alternatively, the heat flux or the rate of evaporation). Information on convection morphology is obtainable from linear stability theory, as has already been shown by Rayleigh. Thus, if we *assume* a type of horizontal pattern (i.e., rolls, rectangles, triangles, hexagons, etc.) and if we *assume* that the final structure is simply the amplification of the fastest-growing mode of the initial infinitesimal disturbance (without change in wavelength), then the horizontal size of the structural unit or "cell" (roll, rectangle, hexagon, etc.) can be determined from the results of the pertinent linear stability theory.

For example, Rayleigh first assumed the horizontal structure to be rectangular (including two-dimensional rolls as a limiting case), and his final governing equations included the parameter $\tilde{a}^2$ which, under the assumption of a rectangular pattern, became the sum of the squares of the dimensionless wave numbers of the disturbance mode along each of a pair of mutually perpendicular axes oriented arbitrarily in the horizontal plane. The critical value of R, i.e., the smallest eigenvalue, was found for each given $\tilde{a}$, and the $\tilde{a}$ yielding the smallest value of R was taken as the parameter describing the

wavelength of the final convection pattern. In particular, if the structure is one of squares, then

$$\tilde{a} = 2\sqrt{2}\pi h/\lambda$$

where λ is the length of a diagonal (A4). If the structure is one of rolls,

$$\tilde{a} = \frac{2\pi h}{\lambda}$$

where λ is the width of a roll. The parameter "$\tilde{a}$" is therefore a by-product of any calculation yielding the critical Rayleigh or Thompson number, and values of $\tilde{a}$ thus determined are tabulated in Table VII for various sets of boundary conditions.

TABLE VII

DIMENSIONLESS CRITICAL WAVE NUMBER FOR THE RAYLEIGH PROBLEM

Type of boundary conditions	Solved by	$\tilde{a}$
Free-free	Rayleigh (R1), 1916	2.22
Solid-solid	Jeffreys (J4), 1928	π
	Pellew and Southwell (P3), 1940	3.13
Solid-free	Pellew and Southwell (P3), 1940	2.68

For other types of patterns, we recall that the complete governing equation (or set of equations) is (are) reduced to an ordinary differential equation involving $\tilde{z}$ only, by means of separation of variables. However, the equation in $\tilde{x}$ and $\tilde{y}$, which was set aside since we considered only the equation in $\tilde{z}$ for determining the critical stability parameter, also involved $\tilde{a}$ and became

$$\frac{\partial^2 u_z^{\dagger}(\tilde{x}, \tilde{y})}{\partial \tilde{x}^2} + \frac{\partial^2 u_z^{\dagger}(\tilde{x}, \tilde{y})}{\partial \tilde{y}^2} = -\tilde{a}^2 u_z^{\dagger}(\tilde{x}, \tilde{y}) \tag{46}$$

where "$\dagger$" denoted a function of $\tilde{x}$ and $\tilde{y}$ only.

Equation (46) is to be solved subject to the requirement that the cylindrical cell walls, i.e., the partitions separating the contiguous cells, be surfaces of symmetry, which in turn requires that on the cell wall the normal component of grad (u_z) [or equivalently of grad (T), as shown by Pellew and Southwell (P3)] should vanish. Therefore

$$\mathbf{n} \cdot \text{grad}\,(u_z) = 0 \tag{47}$$

$\mathbf{n}$ being the outward unit normal to the cell wall. Equation (46) has a solution

for every possible periodic structure. However, if the resulting pattern is to be one of regular polygons, we must limit our consideration to squares, triangles, and hexagons. For squares, the solution to Eq. (46) subject to (47) is

$$u_z^{\dagger}(\tilde{x}, \tilde{y}) = \cos\left(\frac{2\pi h}{\lambda}\tilde{x}\right)\cos\left(\frac{2\pi h}{\lambda}\tilde{y}\right) \tag{48}$$

where λ is the wavelength of the disturbance in both the x and y directions, so that

$$\tilde{a}^2 = 4\pi^2\left[2\left(\frac{h}{\lambda}\right)^2\right] \quad \text{or} \quad \lambda = \frac{2\sqrt{2\pi h}}{\tilde{a}} \tag{49}$$

A plot of Eq. (48) will show λ to be the diagonal of the squares.

The entire flow for the marginal state may now be constructed. The z component of the velocity is given by

$$u_z = u_z^* \cos\left(\frac{2\pi h}{\lambda}\tilde{x}\right)\cos\left(\frac{2\pi h}{\lambda}\tilde{y}\right) \tag{50}$$

and the velocity components u_x and u_y may be recovered as follows: By eliminating p between the first and second of (25) and by dropping the term $\partial/\partial\tilde{t}$, there results

$$\text{div grad}\left(\frac{\partial u_y}{\partial\tilde{x}} - \frac{\partial u_x}{\partial\tilde{y}}\right) = 0 \tag{51}$$

while, because of the continuity equation,

$$-\left(\frac{\partial u_x}{\partial\tilde{x}} + \frac{\partial u_y}{\partial\tilde{y}}\right) = \frac{\partial u_z}{\partial\tilde{z}} \tag{52}$$

Eqs. (51) and (52) may be uncoupled next by letting

$$u_x \equiv -\frac{\partial\varphi}{\partial\tilde{x}} - \frac{\partial\psi}{\partial\tilde{y}}; \qquad u_y \equiv -\frac{\partial\varphi}{\partial\tilde{y}} + \frac{\partial\psi}{\partial\tilde{x}} \tag{53}$$

so that

$$\text{div grad}\left(\frac{\partial^2\psi}{\partial\tilde{x}^2} + \frac{\partial^2\psi}{\partial\tilde{y}^2}\right) = 0 \tag{54}$$

$$\frac{\partial^2\varphi}{\partial\tilde{x}^2} + \frac{\partial^2\varphi}{\partial\tilde{y}^2} = \frac{\partial u_z}{\partial\tilde{z}} \tag{55}$$

which may be solved separately for φ and ψ. u_x and u_y are then recovered from Eq. (53). In this way streamlines and potential lines may be drawn as is shown in Fig. 24 for hexagons.

The flow characterizing hexagons is of greater interest because this seems experimentally to be the preferred form. Christopherson (C4), motivated by the work of Pellew and Southwell, was the first to obtain an exact solution to Eq. (46) for hexagons, which is

$$u_z\dagger = \tfrac{1}{3}[u_z\dagger]^0\left\{2\cos\frac{2\pi h}{\lambda\sqrt{3}}\,\tilde{x}\cos\frac{2\pi h}{3\lambda}\,\tilde{y} + \cos\frac{4\pi h}{3\lambda}\,\tilde{y}\right\} \tag{56}$$

where $[u_z\dagger]^0$ is the undetermined value of u_z at the origin, i.e., the center of the cell. This result clearly points out the fact that this linearized treatment

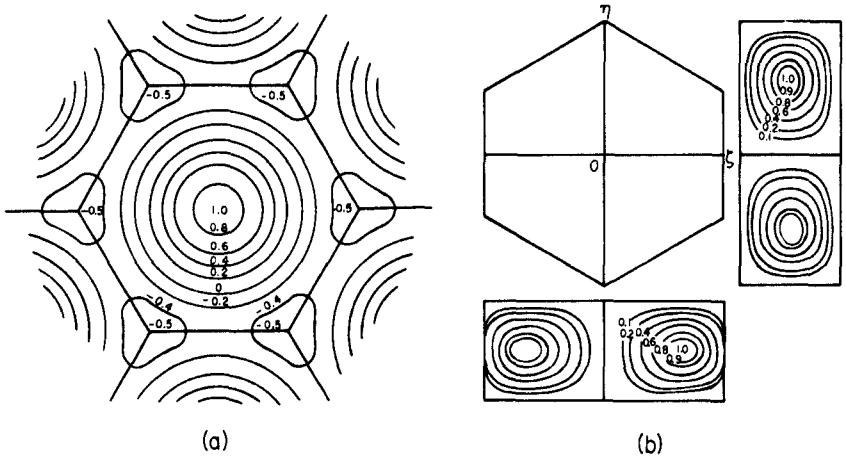

FIG. 24. Streamlines for the stationary marginal state in hexagonal cells: (a) lines of constant u_z* (P3) (courtesy of the Royal Society); (b) side views of streamlines (R3) (courtesy of American Institute of Physics).

cannot tell us anything about the amplitudes or even the direction (sign) of the flow.

Christopherson's solution was generalized in 1960 by Bisshop (cf. C3), who obtained an expression which presumably includes all solutions to Eq. (46) with the required periodicity. The details of the integration to obtain streamlines for hexagonal cells are given by Reid and Harris (R3) and by Chandrasekhar (C3).

It must be remembered, however, that the above methods for calculating cellular flow patterns are valid only for infinitesimal amplitudes, because linear theory (which requires that disturbance flows grow exponentially without limit) cannot by itself predict the final steady flows which are established. On the other hand, flows of macroscopic amplitudes would require consideration of the nonlinear terms in the equations of motion and perhaps the variation of fluid properties with temperature. Still, researchers have persisted in

comparing their experimental cell sizes with the values obtained from linear stability theory, and in some cases have obtained striking, but meaningless, agreement as in Bénard's case (B8, B9). Once again, the assumption which is implicit in using linear theory to predict cell sizes is that, whatever other effects nonlinearity may have on the disturbance flow as it grows, the wavelength will remain unchanged. This assumption appears to be as difficult to correct as it is easy to criticize.

D. Nonlinear Theory

It is in the discussion of the morphology of the convection that the need for consideration of the nonlinear aspects of the theory becomes apparent. The occurrence of instability in a fluid layer which is isolated (to a degree readily attainable in the laboratory) from all but very small disturbances has been successfully predicted by the linear theory, so that the nonlinear aspects of the *stability problem* (i.e., the stability of the system toward *finite* rather than infinitesimal disturbances) have received little attention. But, unless we are willing to make the "constant wavelength" assumption stated above, linear theory reveals nothing at all about the morphology; while if we do make this assumption, all that we can calculate is the cell size for some assumed structure, and the corresponding streamlines for the marginal flow. Thus it is the purpose of nonlinear theory to provide answers to questions such as those listed below.

(*1*) What *structure* (squares, triangles, hexagons, etc.) will be established at steady state?

(*2*) What *direction* will the flow assume (up in the cell centers and down at the sides or vice versa?)

(*3*) What will be the *cell size of the final steady-state* configuration for Rayleigh (or Thompson) numbers in excess of the critical?

(*4*) What will be the *amplitude* of the final steady-state velocity and temperature disturbance for Rayleigh (or Thompson) numbers in excess of the critical?

(*5*) How are *heat and mass transfer rates* related to the Rayleigh (or Thompson) numbers in excess of the critical?

So far, the general point of departure for the nonlinear analyses attempted has been not the set of equations of motion in their complete form, but rather the set that results by neglecting the temperature dependence of all fluid properties except density, and also the dissipation of kinetic energy. This is known as the Boussinesq approximation. Using the Boussinesq equations, Woronetz (W1) was able in 1934 to obtain expressions for the velocity perturbations in a fluid confined between coaxial rotating cylinders or spheres which were maintained at different temperatures. Volkovisky (V3) used the

Boussinesq equations in 1939 to obtain an expression for the velocity along a filament of fluid rising above a point or line heat source placed at the bottom of a fluid layer.

Cellular convection was not treated until 1952 when Pillow (P4) formulated the nonlinear problem for two-dimensional flow between two horizontal plates. He obtained steady velocity profiles for the two-dimensional rolls by neglecting the effects of viscosity and heat conduction except in the region very near the boundaries. Using an approximate theory, he predicted a 5/4-power dependence of heat transfer rate on the temperature difference, which is the proportionality found experimentally.

Gor'kov (G2), in 1957, and Malkus and Veronis (M1), in 1958, succeeded in calculating the steady-state amplitude, as a function of the Rayleigh number, for a given cellular pattern and wavelength using the time-independent Boussinesq equations. A perturbation technique was employed in which the variables were expanded in terms of an amplitude parameter, ε, such as

$$u_z = \hat{u}_z + \varepsilon(\hat{u}_{z_1} + \varepsilon\hat{u}_{z_2} + \varepsilon^2\hat{u}_{z_3} + \cdots) \tag{57}$$

The Rayleigh number was also increased (holding $\tilde{a}$ constant) from its critical value according to

$$R = R_c + \varepsilon R_1 + \varepsilon^2 R_2 + \cdots \tag{58}$$

and a solution was obtained for the case of two free boundaries by retaining terms at least as far as ε^2.

In 1960, Stuart and Watson (cf. S12) examined the same problem using the time-dependent Boussinesq equations and obtained a solution which converged to that of Malkus and Veronis as time approached infinity, thus demonstrating that under unstable conditions a differential disturbance can indeed lead to finite amplitude steady convection.

For the case of two-dimensional roll cells, Malkus and Veronis also performed calculations on the heat transfer rate by using an approximate technique that they considered as being within 2 percent of the exact value, for Rayleigh numbers up to three times the critical. In accordance with experiment, their results show a 5/4-power dependence of heat transfer rate on temperature difference (or a 1/4-power dependence of Nusselt number on the Rayleigh number).

Kuo (K2) has recently obtained a solution to the nonlinear equations of cellular convection by expanding the dependent variables in series of orthogonal functions and by expanding the coefficients of these functions in a power series of an amplitude parameter. His solution also predicts a heat transfer rate proportional to the 5/4 power of the temperature difference.

The problem of cell shape was also treated by Malkus and Veronis, who suggested a criterion based on maximum vertical heat transport. For the case

of two free boundaries, this criterion led to square or rectangular cells. By considering the temperature dependence of viscosity, Palm (P1) showed in 1960 that there is a natural tendency toward hexagonal cells in the steady state.

The question concerning the direction which the cellular flow would assume (i.e., whether it would fall or rise in the cell center) was raised by Graham (G3) in 1933, when he noted that in cellular convection in gases the warm fluid would rise along the periphery of the cells and fall at the center, in contrast to all of the observations in liquids where the flow was always in the opposite sense. Graham suggested that the fluid in the cell center would flow in the direction of increasing kinematic viscosity. The nonlinear analysis by Palm (P1) in 1960, which took into account the temperature dependence of the viscosity, confirmed Graham's suggestion.

As far as is known to the authors, none of the nonlinear theories has been able to predict a preferred wavelength. Also it appears that no nonlinear analysis has been attempted for surface tension driven flows. Convection in deep layers of fluid has also never been treated theoretically.

In ending this section it is appropriate to point out the recent review of "Nonlinear Effects in Hydrodynamic Stability" by Stuart (S12), from which some of the foregoing remarks were drawn.

ACKNOWLEDGMENT

This work was supported in part by grants from the Petroleum Research Fund administered by the American Chemical Society, and from the Office of Saline Water.

Nomenclature

a	Wave number
c_p	Specific heat at constant pressure
c_v	Specific heat at constant volume
D	Differential operator, d/dz
$\mathbf{e}$	Unit vector
$\mathbf{f}$	Body force
g	Acceleration of gravity
h	Thickness of fluid layer
j	Integer
K	Radiation constant
k	Thermal conductivity
l	Wave number
m	Wave number
$\mathbf{n}$	Unit normal vector
N_e	Evaporation number
p	Pressure
q	Growth constant
R	Rayleigh number
s	Roots of auxiliary equation
T	Temperature
t	Time
$\mathbf{u}$	Velocity
u, v, w	Velocity components
x, y, z	Cartesian coordinates

GREEK LETTERS

α	Volumetric coefficient of thermal expansion
β	Temperature gradient
Δ	Difference
ε	Amplitude parameter
θ	Angular deflection
κ	Thermal diffusivity
λ	Wavelength
μ	Viscosity
ν	Kinematic viscosity

ρ Density
σ Surface Tension
τ Stress vector
φ Potential function
ψ Stream function
Ω Angular velocity

SUBSCRIPTS

b Bottom
c Critical
o Refers to initial state
s Surface
x, y, z Refers to Cartesian coordinates

SUPERSCRIPTS

~ Dimensionless quantity
* Refers to initial state
^ Perturbation
* z Dependence
† x, y Dependence

REFERENCES

A1. Adamson, A. W., "Physical Chemistry of Surfaces," Vol. I. Reinhold, New York, 1963.
A2. Avsec, D., *Compt. Rend.* **203**, 556 (1936).
A3. Avsec, D., *Compt. Rend.* **206**, 40 (1938).
A4. Avsec, D., *Publ. Sci. Tech. Min. Air (France)* **155** (1939).
B1. Batchelor, G. K., *Quart. J. Roy. Meteorol. Soc.* **80**, 335 (1954).
B2. "Schlieren Techniques for the Quantitative Study of Gas Mixing." Battelle Mem. Inst., Columbus, Ohio, Project Rand, R-164, 1949.
B3. Bell, S. H., *J. Oil Colour Chemists Assoc.* **35**, 373 (1952).
B4. Bénard, H., *Rev. Gen. Sci. Pures Appl. Bull. Assoc. Franc. Avan. Sci.* **11**, 1261 (1900).
B5. Bénard, H., *Rev. Gen. Sci. Pures Appl. Bull. Assoc. Franc. Avan. Sci.*, **11**, 1309 (1900).
B6. Bénard, H., *Ann. Chim. Phys.* [7] **23**, 62 (1901).
B7. Bénard, H., *Compt. Rend.* **154**, 260 (1912).
B8. Bénard, H., *Compt. Rend.* **185**, 1109 (1927).
B9. Bénard, H., *Compt. Rend.* **185**, 1257 (1927).
B10. Bénard, H., *Bull. Soc. Franc. Phys.* **266**, 1125 (1928).
B11. Bénard, *H.*, *Compt. Rend.* **201**, 1328, (1935).
B12. Berg, J. C., Ph.D. Dissertation, University of California, Berkeley, California, 1964.
B12a. Berg, J. C., unpublished experiments (1964).
B13. Berg, J. C., and Acrivos, A., *Chem. Eng. Sci.* **20**, 737 (1965).
B14. Block, M. J., *Nature* **178**, 650 (1956).
B15. Boys, C. B., "Soap Bubbles and the Forces which Mould Them." Doubleday, New York, 1959.
B16. Brown, S. C., *Daedalus* **86**, 340 (1957).
B17. Brunt, D., *Proc. Roy. Soc.* **A124**, 201 (1929).
C1. Chandra, K., *Proc. Roy. Soc.* **A164**, 231 (1938).
C2. Chandrasekhar, S., *Daedalus* **86**, 323 (1957).
C3. Chandrasekhar, S., "Hydrodynamic and Hydromagnetic Stability." Oxford Univ. Press, London and New York, 1962.
C4. Christopherson, D. G., *Quart. J. Math.* **11**, 63 (1940).
D1. Dauzère, C., *J. Phys.* [4] **6**, 892 (1907).
D2. Dauzère, C., *J. Phys.* [4] **7**, 930 (1907).
D3. Dauzère, C., *Compt. Rend.* **154**, 974 (1912).
D4. Dauzère, C., *Compt. Rend.* **155**, 394 (1912).
D5. Dauzère, C., *Compt. Rend.* **156**, 218 (1913).
D6. Dauzère, C., *Compt. Rend.* **156**, 1228 (1913).
E1. Ewing, G., and McAllister, E. D., *Science* **131**, 1374 (1960).
G1. Gibbs, J. W., "Scientific Papers," Vol. I. Dover, New York, 1961.

G2. Gor'kov, L. P., *Soviet Phys. JETP (English Transl.)* **6**, 311 (1958).
G3. Graham, A., *Phil. Trans. Roy. Soc.* **A232** 285, (1933).
H1. Hershey, A. V., *Phys. Rev.* **56**, 204 (1939).
H2. Hickman, K. C. D., *Ind. Eng. Chem.* **44**, 1892 (1952).
H3. "High Speed Aerodynamics and Jet Propulsion," Vol. IX, Princeton Univ. Press, Princeton, New Jersey, 1954, pp. 26–46.
H4. Holder, D. W., and North, R. J., *AGARD Rept.* (1956).
H5. Hommelen, J., *J. Colloid Sci.* **14**, 385 (1959).
J1. Jarvis, N. L., *J. Colloid Sci.* **17**, 512 (1962).
J2. Jarvis, N. L., Timmons, C. O., and Zisman, W. A., *in* "Retardation of Evaporation, by Monolayers" (V. K. La Mer, ed.), pp. 41–58. Academic Press, New York, 1962.
J3. Jeffreys, H., *Phil. Mag.* [7] **2**, 833 (1926).
J4. Jeffreys, H., *Proc. Roy. Soc.* **A118**, 195 (1928).
J5. Jeffreys, H., *Quart. J. Mech.* [3] **4**, 283 (1951).
J6. Jenkins, F. A., and White, H. E., "Fundamentals of Optics," 3rd. ed. McGraw-Hill, New York, 1957.
K1. Knacke, O., and Stranski, I. N., *Prog. Metal Phys.* **5**, 181.
K2. Kuo, H. L., *J. Fluid Mech.* **10**, 611 (1961).
L1. Langmuir, I., and Langmuir, D. B., *J. Phys. Chem.* **31**, 1719 (1927).
L2. Levengood, W. C., *Astrophys. J.* **129**, 483 (1959).
L3. Lin, C. C., "The Theory of Hydrodynamic Stability." Cambridge Univ. Press, London and New York, 1955.
L4. Linde, H., Pfaff, S., and C. Firkel, *Z. Physik. Chem. (Leipzig)* **224**, 72 (1964).
L5. Loewenthal, M., *Phil. Mag.* [7] **12**, 462 (1931).
L6. Low, A. R., *Proc. Roy. Soc.* **A125**, 180 (1929).
L7. Low, A. R., *Proc. 3rd Intern. Congr. Appl. Mech.*, 1929, Vol. I, pp. 109-120. Norsted & Söner, Stockholm, 1930.
L8. Low. A. R., and Brunt, D., *Nature* **115**, 299 (1925).
L9. Luntz, M., *Compt. Rend.* **204**, 547 (1937).
M1. Malkus, W. V. R., and Veronis, G., *J. Fluid Mech.* **4**, 225 (1958).
M2. Marangoni, C., *Nuovo Cimento* [2] **16**, 239 (1871).
M3. Marangoni, C., *Nuovo Cimento* [3] **3**, 97 (1878).
M4. Miner, R. W., *Ann. N.Y. Acad. Sci.* **48**, (1947).
M5. Mysels, K. J., *Science* **129**, 96 (1959).
N1. Nield, D. A., *J. Fluid Mech.* **19**, 341 (1964).
O1. Orchard, S. E., *Appl. Sci. Res.* **A11**, 451 (1963).
O2. Orell, A., and Westwater, J. W., *Chem. Eng. Sci.* **16**, 127 (1961).
O3. Orell, A., and Westwater, W. J., *A.I.Ch.E. (Am. Inst. Chem. Engrs.)* **8**, 350 (1962).
P1. Palm, E., *J. Fluid Mech.* **8**, 183 (1960).
P2. Pearson, J. R. A., *J. Fluid Mech.* **4**, 489 (1958).
P3. Pellew, A., and Southwell, R. V., *Proc. Roy. Soc.* **A176**, 312 (1940).
P4. Pillow, A. F., *Aeronaut. Res. Rept. Australia* **A79**, 1 (1952).
R1. Rayleigh, Lord, *Phil. Mag.* [6] **32**, 529 (1916).
R2. Reid, W. H., and Harris, D. L., *Phys. Fluids* **1**, 102 (1958).
R3. Reid, W. H., and Harris, D. L., *Phys. Fluids* **2**, 716 (1959).
R4. Rumford, Count, "Complete Works," Vol. 2, pp. 239 ff. Am. Acad. Arts Sci., Boston, Massachusetts, 1870.
S1. Sartory, G., *Compt. Rend.* **208**, 327 (1939).
S2. Saunders, D. A., Fishenden, M., and H. D. Mansion, *Engineering, London* **139**, 483 (1935).

S3. Schardin, H., "Toepler's Schlieren Method: Basic Principles for Its Use and Quantitative Evaluation." David Taylor Model Basin, U.S. Navy Transl. No. 156, 1947.
S4. Schmidt, R. J., and Milverton, S. W., *Proc. Roy. Soc.* **A152**, 586 (1935).
S5. Schmidt, R. J., and Saunders, D. A., *Proc. Roy. Soc.* **A165**, 216 (1938).
S6. Scriven, L. E., and Sternling, C. V., *Nature* **187**, 186 (1960).
S7. Scriven, L. E., and Sternling, C. V., *J. Fluid Mech.* **19**, 321 (1964).
S8. Sellin, R. H. J., *J. Sci. Instr.* **40**, 355 (1963).
S9. Silveston, P. L., *Forsch. Ing. Wes.* **24**, 29 and 59 (1958).
S10. Spangenberg, W. B., and Rowland, W. R., *Phys. Fluids* **4**, 743 (1961).
S11. Sparrow, E. M., Goldstein, R. J., and Jonsson, V. K., *J. Fluid Mech.* **18**, 513 (1964).
S12. Stuart, J. T., *Proc. 10th Intern. Congr. Appl. Mech.*, Stresa, Italy, 1960, p. 63, Elsevier, Amsterdam, 1962.
S13. Sutton, O. G., *Proc. Roy. Soc.* **A204**, 297 (1950).
T1. Taylor, G. I., *Phil. Trans. Roy. Soc.* **A223**, 289 (1923).
T2. Terada, T., *Rept. Aeronaut. Res. Inst. Tokyo* **3**, 3(1928); **4**, 448 (1929).
T3. Thompson, J. J., *Phil. Mag.* [4] **10**, 330 (1855)
T4. Thompson J. J., *Proc. Roy. Phil. Soc. Glasgow.* **13**, 464 (1882).
T5. Tomlinson, C., *Phil. Mag.* [4] **27**, 528 (1864).
T6. Tomlinson, C., *Phil. Mag.* [4] **38**, 409 (1869).
V1. Varley, C., *Trans. Roy. Soc. Arts Sci. Mauritius* **50**, 190 (1836).
V2. Vernotte, P., *Compt. Rend.* **202**, 119 (1936).
V3. Volkovisky, V., *Compt. Rend.* **200**, 1285 (1935).
V4. Volkovisky, V., *Publ. Sci. Tech. Min. Air (France)* **151**, 1 (1939).
V5. Vidal, A., and Acrivos, A., *Phys. Fluids* **9**, 615 (1966).
W1. Woronetz, C., *Publ. Sci. Tech. Min. Air (France), Notes Tech.* **60**, 1 (1934).